HATHOR for single top-quark production: Updated predictions and uncertainty estimates for single top-quark production in hadronic collisions

P. Kant, O.M. Kind, T. Kintscher, T. Lohse, T. Martini, S. Mölbitz, P. Rieck, and P. Uwer

Humboldt-Universität zu Berlin, Institut für Physik, Newtonstraße 15, 12489 Berlin, Germany

May 20, 2015

We present updated predictions for single top-quark production in hadronic collisions. The analysis is based on next-to-leading order QCD calculations. The input parameters are fixed to recent measurements. We compare different PDF sets and investigate the related uncertainties. The impact of uncalculated higher orders is estimated using an independent variation of the renormalisation and factorisation scale. The theoretical predictions are compared with recent measurements from Tevatron and LHC. Furthermore, the cross section measurements are used to estimate the top-quark mass. To perform the analysis we extended the publicly available HATHOR program to single top-quark production. We thus provide a unified framework for the fast numerical evaluation of total cross sections for top-quark production, which may be used for example in Standard Model fits. For future extensions towards NNLO accuracy, we include already all scale dependent terms at NNLO. We briefly describe how to use the program and provide all required tools to repeat the aforementioned analysis.

1 Introduction

In high energetic hadron-hadron collisions, top quarks are produced dominantly in pairs via the strong interaction, but also singly through the weak interaction. Being of electroweak origin, the rates for single top-quark production are evidently reduced compared to top-quark pair production. With cross sections of about one third of the respective cross sections for inclusive top-quark pair production, still a significant number of single top-quark events is produced at the Tevatron and the LHC. The experimental analysis of single top-quark production is, however, challenging owing to the complicated event signature and sizeable backgrounds. Despite these complications, single top-quark production is highly interesting for various reasons: it provides a direct probe of the Wtb coupling which is sensitive to many models of physics beyond the Standard Model (SM) [1, 2]. In the SM, single top-quark production allows a precise

study of the $V-A$ structure of the charged current interaction. In addition, it gives a direct handle to the Cabibbo-Kobayashi-Maskawa (CKM) matrix element V_{tb} which is otherwise only measured indirectly. Furthermore, single top-quark production provides a unique source of highly polarised top quarks and may also offer valuable information to constrain the b-quark content in the proton.

(a) *t*-channel production   **(b)** Associated Wt production   **(c)** *s*-channel production
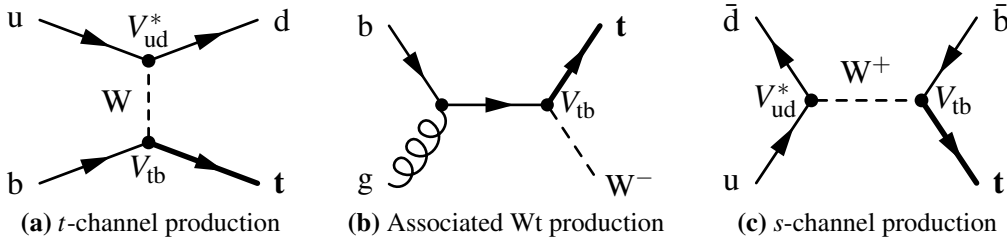
Figure 1: Feynman diagrams in leading order for the dominant hard scattering processes in the three subprocesses of single top-quark production.

In Fig. 1, sample diagrams for single top-quark production in the SM are shown. The *t*-channel production dominates at both colliders, Tevatron and LHC. The next-to-leading order (NLO) QCD corrections for the *t*-channel have been calculated for the inclusive cross section in Refs. [3–5]. In Refs. [6–8] fully differential results are presented, which are extended in Refs. [9–11] to include also the semi-leptonic decay of the top quark. In Ref. [12] the fixed-order predictions are combined with parton shower results using the MC@NLO framework. A similar study including also the *s*-channel contributions using the POWHEG framework is presented in Ref. [13].

At the LHC, the associated Wt production represents the second important production channel; at the Tevatron this channel contributes only at the level of a few per cent. The NLO corrections for the associated production are given in fully differential form in Refs. [14, 15]. At NLO, associated Wt production interferes with leading order $t\bar{t}$ production and the subsequent decay $\bar{t} \rightarrow W^-\bar{b}$. The splitting $g \rightarrow b\bar{b}$ in the signal process prefers a small transverse momentum $p_t^{\bar{b}}$ of the outgoing $\bar{b}$. This is not the case for the $\bar{b}$ produced in the $\bar{t}$ decay. One method to suppress the contribution from $t\bar{t}$ production and to disentangle to some extent the two processes is thus to apply a cut on the transverse momentum of the $\bar{b}$ in the final state. Typically, values lower than $25 - 50$ GeV are used for this cut [16]. Alternatively, one might use diagram removal or diagram subtraction techniques to disentangle top-quark pair production and single top-quark production [17]. For associated production, the semi-leptonic top-quark decay has been considered in Ref. [18]. Recently, the fixed order NLO corrections were also combined with the parton shower. Two implementations have been presented: one in the MC@NLO framework [19] and another in the POWHEG framework [20].

The third channel, the *s*-channel, is the second important channel at the Tevatron while it gives only a small contribution at the LHC. The NLO corrections for the inclusive *s*-channel production are given in Ref. [21]. Fully differential results have been published together with the results for the *t*-channel in Ref. [6]. Results including the top-quark decay are given in Refs. [9, 22].

In Refs. [23, 24], *t*-channel single top-quark production has been studied in the four-flavour scheme. In this approach the b-quark is not considered as part of the proton. The leading

order process is thus a two-to-three process. The naive expectation is that the two schemes should give similar results as long as effects of the finite b-quark mass can be neglected and the observables are not affected by $\ln(m_b)$ terms. Indeed, the authors of Refs. [23, 24] find a reasonable agreement between the two approaches.

Beyond fixed order in QCD, also the impact of large logarithmic corrections due to soft gluon contributions have been studied in detail. Being universal, these corrections can be partially resummed to all orders in perturbation theory. Alternatively one may use the universal terms to construct an ansatz for the yet uncalculated next-to-next-to-leading oder (NNLO) corrections. Both approaches are extensively discussed in the literature. For more details we refer to Refs. [15, 25–30]. Very recently partial NNLO results for single top-quark production in the t-channel have been presented [31]. More precisely, the NNLO vertex corrections and the related real corrections are calculated. Double-box topologies are not included. In Ref. [32] the reduction to master integrals is presented for the full set of two-loop corrections. Unfortunately, the highly non-trivial two-loop master integrals are still unknown.

The vast amount of available literature documents a solid theoretical understanding of single top-quark production. Despite the non-negligible event rates, it took however some time to discover single top-quark production in hadronic collisions. It was first observed in p$\bar{\text{p}}$ collisions at the Tevatron by the CDF and D∅ collaborations [33, 34]. In pp collisions, single top-quark production was discovered in the t-channel by the ATLAS and CMS collaborations for a centre-of-mass energy of 7 TeV [35, 36]. In addition, evidence for the associated Wt production was reported in Refs. [37, 38] and later observed by the CMS collaboration with a significance of more than five standard deviations [39]. For s-channel production, so far only upper limits are given by the LHC experiments [40, 41], while the Tevatron experiments recently reported the observation of the s-channel [42].

The aforementioned experimental results reflect just the beginning of a growing activity. Refined experimental analysis in combination with larger data samples will lead to a steadily increasing precision of the experimental studies. To make optimal use of these results in the context of precision tests of the SM and New Physics searches, a detailed comparison with theoretical predictions is mandatory. For differential distributions, publicly available tools exist to perform such a comparison at NLO accuracy. At the parton level, for example, the *Monte Carlo for FeMtobarn processes* (MCFM) [9, 18, 23, 43] represents a convenient framework. For the t and the s-channel also the program ZTOP [7] can be used. The Monte Carlo generators MC@NLO [12, 19] and POWHEG [13, 20] may be used to incorporate also the effect of the parton shower. As a matter of fact, these tools can also be used to calculate predictions for inclusive cross sections. However, since they are designed for differential distributions, this requires in general a phase space integration which is done numerically and may lead to an increased runtime. Detailed investigations of inclusive cross sections like for example studies of renormalisation and factorisation scale dependencies or uncertainty studies due to the parton distribution functions (PDF) may be limited by the available computing resources. One aim of this article is to provide a publicly available tool dedicated to the calculation of inclusive cross sections, similar to what has been done for top-quark pair production [44–47]. Using inclusive cross sections at the parton level as input for the convolution with the PDFs, the numerical phase space integration is avoided. This approach is implemented in the HATHOR program which is thus extended to also allow state of the art theoretical predictions for hadronic single top-quark production. As an application, we investigate in detail the impact of PDF uncer-

tainties and study the independent variation of the renormalisation and the factorisation scale. Future applications could be fits of the b-PDF or a global data analysis in the context of the SM. In the next section we outline the theoretical setup, give a short description of the program and discuss its validation. Section 3 outlines how to use the HATHOR program. In Sec. 4 the program is applied to study in detail theoretical uncertainties due to factorisation and renormalisation scale variations and parton distribution functions. In addition, the theoretical predictions are compared with recent measurements. Section 5 summarises the main results of this article.

2 Theoretical setup

Throughout this article, we restrict ourselves to the inclusive cross section for single top-quark production. The top-quark mass m_t is renormalised in the on-shell scheme. In the QCD improved parton model, the inclusive cross section for single top-quark production is calculated according to

$$\sigma_{\text{had}}(s) = \sum_{i,j} \iint \mathrm{d}x_1 \mathrm{d}x_2 \, F_{i/h_1}(x_1, \mu_{\text{F}}) \, F_{j/h_2}(x_2, \mu_{\text{F}}) \, \hat{\sigma}_{ij}(\hat{s}; \alpha_{\text{s}}(\mu_{\text{R}}), \mu_{\text{F}}), \tag{1}$$

where s is the hadronic centre-of-mass energy squared. The factorised cross section for the hard scattering of two incoming partons i and j with partonic centre-of-mass energy squared $\hat{s} = x_1 x_2 s$ is described by $\hat{\sigma}_{ij}$. The renormalisation and factorisation scales are denoted by μ_{R} and μ_{F}, respectively. The parton distribution functions are given by $F_{i/h}(x, \mu_{\text{F}})$. Qualitatively, they describe the probability to find the parton i inside the hadron h with momentum fraction between x and $x + \mathrm{d}x$. The QCD coupling $\alpha_{\text{s}}(\mu_{\text{R}})$ is determined in a scheme with five massless flavours. Note in particular that the b-quark is treated as massless. In the five-flavour scheme, the b-quark in the initial state is described by the appropriate b-PDF. For each production channel the factorised partonic cross section can be expanded in

$$a(\mu_{\text{R}}) = \frac{\alpha_{\text{s}}(\mu_{\text{R}})}{2\pi}. \tag{2}$$

Up to NNLO accuracy the expansion reads:

$$\hat{\sigma}_{ij}(\hat{s}; \alpha_{\text{s}}(\mu_{\text{R}}), \mu_{\text{F}}) = a^k(\mu_{\text{R}})\hat{\sigma}_{ij}^{(0)}(\hat{s}) + a^{k+1}(\mu_{\text{R}})\hat{\sigma}_{ij}^{(1)}(\hat{s}; \mu_{\text{R}}, \mu_{\text{F}}) + a^{k+2}(\mu_{\text{R}})\hat{\sigma}_{ij}^{(2)}(\hat{s}; \mu_{\text{R}}, \mu_{\text{F}}). \tag{3}$$

For s and t-channel production we have $k = 0$, while for the associated production k is equal to 1. For the leading order cross sections $\hat{\sigma}_{ij}^{(0)}$, compact analytic expressions exist and the application of Eq. (1) is straightforward.

2.1 Partonic cross section at NLO

At NLO accuracy, no compact analytic expressions for the inclusive cross sections are available in closed form. Complete NLO calculations have been published. However, these calculations typically involve numerical phase space integrations of virtual and real corrections. The complete code to perform these integrations for all three production channels has been

published for example in the MCFM program. In principle, the program can also be used to evaluate the partonic cross sections for different partonic energies. In practice, the extraction is however non-trivial due to the complicated structure of one-loop calculations and the fact that this option is not intended by the authors of MCFM. The NLO cross section $\hat{\sigma}_{ij}^{(1)}$ includes contributions from virtual corrections σ_{ij}^V, real corrections σ_{ij}^R and the factorisation of initial state singularities σ_{ij}^{fac}. Schematically we may write

$$a^{k+1}(\mu_{\text{R}})\hat{\sigma}_{ij}^{(1)} = \sigma_{ij}^V + \sigma_{ij}^R + \sigma_{ij}^{\text{fac}} \tag{4}$$

$$= \int \mathrm{d}R_n \frac{\mathrm{d}\sigma_{ij}^V}{\mathrm{d}R_n} + \int \mathrm{d}R_{n+1} \frac{\mathrm{d}\sigma_{ij}^R}{\mathrm{d}R_{n+1}} + \int \mathrm{d}x \mathrm{d}R_n \frac{\mathrm{d}\sigma_{ij}^{\text{fac},x}}{\mathrm{d}R_n}, \tag{5}$$

where $\mathrm{d}R_n$ denotes the n particle phase space measure. Each contribution contains soft and collinear singularities which cancel in the sum. To achieve this cancellation, the Catani-Seymour subtraction formalism [48, 49] is employed in MCFM, i.e. local counter terms are added (and subtracted) such that each contribution is rendered finite and the total result remains unchanged. Technically, this introduces additional terms in the calculation which are difficult to identify in a generic NLO code. Furthermore, the factorisation of initial state singularities but also the subtraction formalism, introduce additional convolutions (indicated by the additional x integration in Eq. (5)). These convolutions obscure further the correct identification of the partonic centre-of-mass energy which is however required for the calculation of the partonic cross sections.

To obtain the partonic cross sections at NLO accuracy, three complementary approaches have been followed in this work. In order to avoid any intervention concerning the MCFM code, the first approach was to run MCFM using pseudo-PDFs which allow for an extraction of the partonic cross section $\hat{\sigma}_{ij}^{(1)}$. For the partonic channel of interest, we use narrow Gaussian distributions as parton distribution functions to probe the partonic cross section $\hat{\sigma}$ at the partonic centre-of-mass energy $\hat{s} = x_0^2 s$. More precisely we set

$$F_{i/\text{h}}(x, \mu_0) = \frac{1}{\sqrt{2\pi}\delta} \exp\left(-\frac{(x-x_0)^2}{2\delta^2}\right), \tag{6}$$

where δ describes the width of the Gaussian distribution. Those PDFs leading to additional partonic channels are set to zero. Using the pseudo-PDFs, we obtain to good approximation

$$\sigma_{\text{had}}(s; \mu_0, \mu_0)|_{\text{pseudo-PDFs}} = \hat{\sigma}_{i,j}(x_0^2 s; \mu_0, \mu_0) + O(\delta^2). \tag{7}$$

The systematic error of the extracted cross section is proportional to the square of the width of the pseudo-PDFs. Further uncertainties arise at the threshold when a part of the pseudo-PDF is essentially cut off and the pseudo-PDF is thus no longer normalized to 1. Within these limitations, a precise extraction of $\hat{\sigma}$ is possible over a wide range of partonic centre-of-mass energies, provided the width δ is chosen small enough. The self consistency can be checked by using different values for δ. Note that the procedure is only applied once for $\mu_{\text{R}} = \mu_{\text{F}} = \mu_0$, since the full renormalisation and factorisation scale (in)dependence can be restored using the renormalisation group equation.

This approach was validated by reproducing the known scaling functions for top-quark pair production. In addition, we applied the method to reproduce the known analytic results for
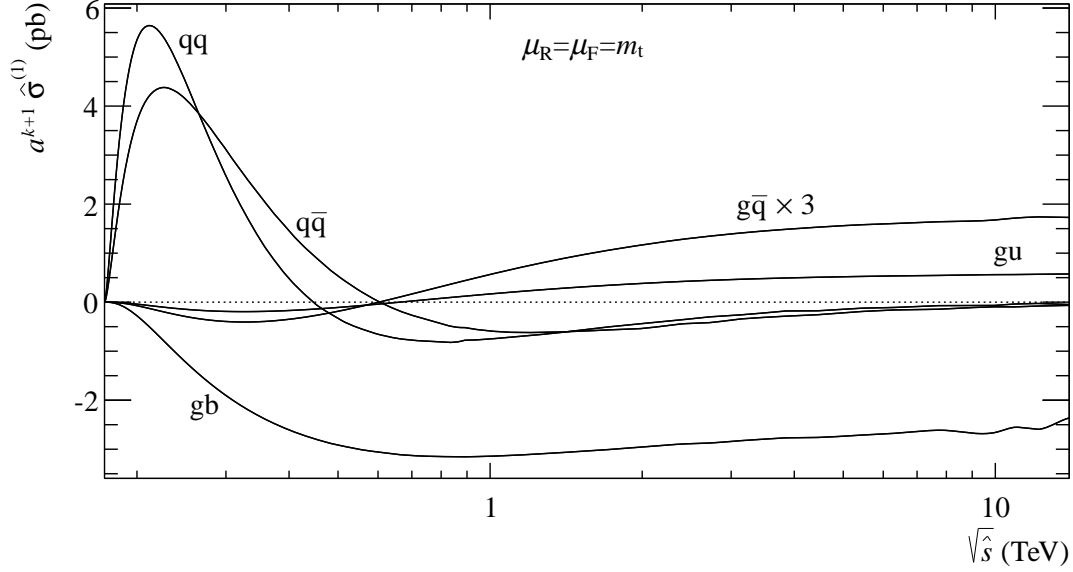
Figure 2: NLO contributions to the partonic cross section for single top-quark production (*t*-channel) as a function of the partonic centre-of-mass energy for a top-quark mass of 172.5 GeV. Both scales μ_R and μ_F are set to the mass of the top quark. Here, q and $\bar{q}$ indicate all applicable flavours for the given channel, whereas u denotes an up or charm quark and b denotes a down-like quark.

single top-quark production in leading-order. Subsequently, the NLO corrections for single top-quark production have been extracted. Close to threshold, where small values of δ are required, a significant numerical effort is necessary since MCFM is not designed to cope with the employed type of PDFs. Despite this drawback, the method is universally applicable to extract partonic cross sections from generic NLO programs without the need to modify the respective programs.

As an alternative approach we have studied the internal structure of MCFM to identify the partonic cross sections. Once this was done, we were able to remove the integration over the parton distribution functions and restrict the numerical integration to the phase space and convolution integrals.[1] Evidently, this approach is numerically much more efficient than using pseudo-PDFs and leads to a shorter runtime and numerically much more precise partonic cross sections. Furthermore, being able to remove the integration over the PDFs analytically eliminates the systematic error associated with the pseudo-PDFs. The downside of this approach is the necessity for considerable changes of the MCFM program.

For a given value of the top-quark mass, the results of these two approaches have been compared for all production channels and all corresponding initial states. All results agree with each other within less than 1 ‰, which proves the correctness of the two methods.

As a third approach, we have written a private code implementing the virtual corrections as given in Ref. [6]. We have restricted ourselves to *s* and *t*-channel production. Again we found perfect agreement with the results extracted using the two methods described above.

In Fig. 2, we show as an example the NLO *t*-channel cross sections for a top-quark mass of $m_t = 172.5$ GeV. The corresponding plots for *s*-channel and Wt production are given in App. B

---

[1]A similar approach is followed in the APPLGRID framework [50].

Variable	Default value	Fixed	Valid range
$\sqrt{s}$	1.96 TeV (p$\bar{\text{p}}$), 8 TeV (pp)	no	any
Colliding hadrons	pp	no	pp, p$\bar{\text{p}}$
Top charge	t	no	t, $\bar{\text{t}}$, t+$\bar{\text{t}}$
$(\hbar c)^2$	3.89379323×10^8 GeV^{2}pb	no	—
$\sin^2 \theta_W$	0.2228972	no	—
$\alpha(m_Z^2)$	$1/132.2332298$	no	—
α_s	depends on chosen PDF	no	any appropriate PDF
m_W	80.385 GeV	yes	—
m_t (pole mass)	(173.5 GeV)	no	165 – 950 GeV
μ_R, μ_F	(m_t)	no	any
CKM matrix	PDG 2012	no	any
$p_t^{\bar{b}}$ (assoc. Wt prod.)	$\leq$ 25 GeV	yes	—
PDF set	(CT10 nlo)	no	any from LHAPDF

Table 1: Collection of all constants and parameter settings of the HATHOR program. Their choice is based on latest world averages [51]. Some of the model parameters can be varied by the user (cf. Sec. 3), while the other values are fixed. Unless otherwise stated, the values in brackets are used throughout the figures in this paper, but they do not have defaults in HATHOR. All PDF sets available in the Les Houches Accord PDF Interface (LHAPDF) [52] can be used. The value for α_s is predetermined by the chosen PDF set. Several PDF groups provide sets with varied α_s values which can be used to study the α_s dependence (see Fig. 8).

(Fig. 10a and Fig. 10b). Note that single top-quark production depends on a variety of input parameters, in contrast to top-quark pair production. While in top-quark pair production it is possible to factor out the top-quark mass and α_s, and define dimensionless scaling functions which depend only on $4m_t^2/\hat{s}$ — allowing to keep the full top-quark mass dependence — this is not possible for single top-quark production. In addition to the top-quark mass, single top-quark production depends also on the W mass. The full mass dependence can thus not be encoded in a one-dimensional function. Furthermore, the cross section depends also on the weak coupling and the CKM matrix elements. This dependence is, however, multiplicative and can be factored out. For the numerical extraction of the partonic cross sections, we have used the present world average [51] for the respective input. In Tab. 1, we show the default values adopted in this work. Since in most cases the dependence on the input parameters is kept in analytic form, their values can be easily changed. An exception is the dependence on the W boson mass. Since the W mass is measured very precisely, we have fixed the value to the current world average value. Possible future changes are expected to be only of the order of a few MeV which will not lead to relevant changes of the cross section for single top-quark production. In case of the top-quark mass, we have repeated the extraction for different input values allowing to change the mass later in a wide range. This does not only allow to study the m_t dependence of cross sections, but also to compute cross sections for electroweak production of hypothetical heavier versions of the top quark. The partonic cross sections have thus been sampled for 18 different values of the top-quark mass and 64 different values of the partonic centre-of-mass energy. Since the energy threshold for any given production

process depends on m_t, the sampling points for the centre-of-mass energy have been chosen individually for each value of the top-quark mass, starting with the production threshold M. For the s and t-channel, M equals m_t, whereas in the case of Wt production $M = m_W + m_t$. The majority of the sampling points is placed close to the threshold and the spacing between adjacent points increases with higher energies. Therefore the resulting grid is not equidistant in $\sqrt{\hat{s}}$. In the calculation of the hadronic cross section, the partonic cross sections are required for arbitrary values of the partonic centre-of-mass energy between the threshold M and the collider energy. To obtain the cross section for intermediate masses and intermediate partonic centre-of-mass energies from the values stored in the two dimensional grid, we use two subsequent interpolations. If the mass does not correspond to one of the values used in the calculation of the grid, we interpolate first in the mass to find the cross section values for the required mass and neighbouring centre-of-mass energies. This first interpolation is polynomial for m_t below 165 GeV and logarithmic above 165 GeV. In a second (polynomial) interpolation in the centre-of-mass energy the cross section for the required centre-of-mass energy is determined. In fact, we do not interpolate in $\hat{s}$ but in $M^2/\hat{s}$.

In order to obtain the total cross section, no kinematic cuts are applied and the entire phase space is included in the integration. However, there is one exception. In the case of the associated production of a W boson and a top quark, the issue of interference with top-quark pair production arises at NLO. For initial states consisting of either a pair of gluons or a pair of quarks, contributions from $t\bar{t}$ production can lead to the same final state. The MCFM program allows to impose a cut on the transverse momentum $p_t^{\bar{b}}$ of the outgoing b-quark, which suppresses the contribution from $t\bar{t}$ production. In concordance with current experimental settings, the suggestion given in Ref. [16] is followed, and an upper limit of $p_t^{\bar{b}} \le 25$ GeV is used.

2.2 Renormalisation and factorisation scale dependence

Having extracted the partonic cross sections at NLO for the renormalisation and factorisation scales equal to the top-quark mass, the scale dependent terms at NLO and NNLO can be derived from the renormalisation group equation. Here, the NNLO scale dependence is calculated as a first step of a possible future extension towards NNLO accuracy (all the scale dependent terms presented in the following are included in the Hathor library, which will be discussed in the next section). For the derivation of the scale dependent terms it is convenient to introduce for each partonic channel scaling functions f_{ij} defined by

$$\hat{\sigma}_{ij} = \rho\, f_{ij}(\rho)\,, \tag{8}$$

with $\rho = M^2/\hat{s}$ as before. The total hadronic cross section is then given by

$$\sigma_{\text{had}}(s; \mu_F, \mu_R) = \frac{M^2}{s} \sum_{i,j} F_{i/h_1} \otimes F_{j/h_2} \otimes f_{ij}\,, \tag{9}$$

where the convolution $\otimes$ is defined through

$$(f \otimes g)(x) = \int dy\, dz\, \delta(x - yz) f(y) g(z) = \int_x^1 \frac{dy}{y} f(y) g\left(\frac{x}{y}\right)\,. \tag{10}$$

8

Using the Dokshitzer-Gribov-Lipatov-Altarelli-Parisi evolution equation of the parton distribution functions,

$$\frac{\mathrm{d}F_i(x,\mu)}{\mathrm{d}\ln(\mu^2)} = a(\mu)\sum_j P_{ij} \otimes F_j(x,\mu),\tag{11}$$

for $\mu = \mu_F = \mu_R$, together with the QCD beta function

$$\frac{\mathrm{d}a(\mu)}{\mathrm{d}\ln(\mu^2)} = -\beta(a) = -a^2\left(\beta_0 + a\beta_1 + \dots\right),\tag{12}$$

with

$$\beta_0 = \frac{1}{2}\left(11 - \frac{2}{3}n_f\right),\quad \beta_1 = \frac{1}{4}\left(102 - \frac{38}{3}n_f\right),$$

and

$$a(\mu_F) = a(\mu_R)\left(1 + \beta_0 L_R a(\mu_R) + \left[\beta_1 L_R + \beta_0^2 L_R^2\right]a(\mu_R)^2 + \dots\right),\tag{13}$$

it is straightforward to derive the general structure of the scale dependent terms:

$$\frac{1}{\rho}\hat{\sigma}^{(0)}(\hat{s};\mu_R,\mu_F) = f^{(0)},\tag{14}$$

$$\frac{1}{\rho}\hat{\sigma}^{(1)}(\hat{s};\mu_R,\mu_F) = f^{(10)} + L_M f^{(11)} + k\beta_0 L_R f^{(0)},\tag{15}$$

$$\frac{1}{\rho}\hat{\sigma}^{(2)}(\hat{s};\mu_R,\mu_F) = f^{(20)} + L_M f^{(21)} + L_M^2 f^{(22)} + k\beta_1 L_R f^{(0)}$$
$$+ \ (k+1)\beta_0 L_R\left(f^{(10)} + L_M f^{(11)}\right) + \tfrac{1}{2}k(k+1)\beta_0^2 L_R^2 f^{(0)},\tag{16}$$

where

$$L_M = \ln\left(\frac{\mu_F^2}{m_t^2}\right)\quad\text{and}\quad L_R = \ln\left(\frac{\mu_R^2}{\mu_F^2}\right).$$

For simplicity we have suppressed the parton indices. Note that the scaling functions $f^{(i)}$ do not depend on μ_R and μ_F. Using

$$P_{ij} = P_{ij}^{(0)} + 4\pi\alpha_s P_{ij}^{(1)} + O(\alpha_s^2),\tag{17}$$

the functions $f^{(11)}, f^{(21)}, f^{(22)}$ are given by

$$f_{ij}^{(11)} = -\sum_{m\in q,\bar{q},g}\left(P_{mi}^{(0)}\otimes f_{mj}^{(0)} + P_{mj}^{(0)}\otimes f_{im}^{(0)}\right) + k\beta_0 f_{ij}^{(0)},\tag{18}$$

$$f_{ij}^{(21)} = -\sum_{m\in q,\bar{q},g}\left(P_{mi}^{(1)}\otimes f_{mj}^{(0)} + P_{mj}^{(1)}\otimes f_{im}^{(0)}\right) + k\beta_1 f_{ij}^{(0)}$$
$$- \sum_{m\in q,\bar{q},g}\left(P_{mi}^{(0)}\otimes f_{mj}^{(10)} + P_{mj}^{(0)}\otimes f_{im}^{(10)}\right) + (k+1)\beta_0 f_{ij}^{(10)},\tag{19}$$

$$2f_{ij}^{(22)} = -\sum_{m\in q,\bar{q},g}\left(P_{mi}^{(0)}\otimes f_{mj}^{(11)} + P_{mj}^{(0)}\otimes f_{im}^{(11)}\right) + (k+1)\beta_0 f_{ij}^{(11)}.\tag{20}$$

The equations (18)–(20) are universally applicable to any process. Within the five-flavour scheme, the sum over q is taken over u,d,s,c,b. In single top-quark production, the cross sections depend on the flavour through the CKM matrix elements. Factoring out the CKM matrix elements, the number of independent cross section evaluations can be greatly reduced. Since the light flavours are not distinguished in the final state it is useful to define

$$\Sigma_q = \begin{cases} \left|V_{qd}\right|^2 + \left|V_{qs}\right|^2 + \left|V_{qb}\right|^2 & q \in \{u,c,t\} \\ \left|V_{uq}\right|^2 + \left|V_{cq}\right|^2 & q \in \{d,s,b\} \end{cases}. \tag{21}$$

Each combination f_{ij} can be split into a CKM-independent part, $\tilde{f}_{ij}$, and a CKM dependent coefficient. The functions $\tilde{f}$ are generic and depend only on the kinematic structure of the corresponding Feynman diagrams. In the s-channel, the scale-independent functions in LO and NLO are defined by:

$$f_{q\bar{q}}^{(0)} = \tilde{f}_{u\bar{d}}^{(0)} \left|V_{q\bar{q}}\right|^2 \Sigma_t, \quad f_{q\bar{q}}^{(i)} = \tilde{f}_{u\bar{d}}^{(i)} \left|V_{q\bar{q}}\right|^2 \Sigma_t, \quad f_{gq}^{(i)} = \tilde{f}_{gu}^{(i)} \Sigma_q \Sigma_t, \quad i \in \{10, 11\}, \tag{22}$$

where in the $q\bar{q}$ case we sum over the initial states $u\bar{d}, u\bar{s}, u\bar{b}, c\bar{d}, c\bar{s}, c\bar{b}$, while in the gq case the sum is taken over $gu, gc, g\bar{d}, g\bar{s}, g\bar{b}$. Having factored out the flavour dependence, the results for $\tilde{f}^{(11)}$ can be simplified to

$$\tilde{f}_{u\bar{d}}^{(11)} = -2P_{qq}^{(0)} \otimes \tilde{f}_{u\bar{d}}^{(0)}, \quad \tilde{f}_{gu}^{(11)} = -P_{qg}^{(0)} \otimes \tilde{f}_{u\bar{d}}^{(0)}. \tag{23}$$

For the t-channel, the dependence on the CKM matrix elements looks as follows:

$$f_{qq'}^{(i)} = \tilde{f}_{bu}^{(i)} \Sigma_q \left|V_{tq'}\right|^2, \qquad\qquad q \in \{u,c\}, q' \in \{b,s,d\}, i \in \{0, 10, 11\}, \tag{24}$$

$$f_{q\bar{q}}^{(i)} = \tilde{f}_{b\bar{d}}^{(i)} \Sigma_{\bar{q}} \left|V_{tq}\right|^2, \qquad\qquad q \in \{b,s,d\}, \bar{q} \in \{\bar{b},\bar{s},\bar{d}\}, \tag{25}$$

$$f_{gq}^{(j)} = \tilde{f}_{gu}^{(j)} \Sigma_q \Sigma_t, \qquad\qquad q \in \{u,c\}, j \in \{10, 11\}, \tag{26}$$

$$f_{gq}^{(j)} = \tilde{f}_{gb}^{(j)} (\Sigma_u + \Sigma_c) \left|V_{tq}\right|^2, \qquad q \in \{d,s,b\} \tag{27}$$

$$f_{g\bar{q}}^{(j)} = \tilde{f}_{g\bar{d}}^{(j)} \Sigma_{\bar{q}} \Sigma_t, \qquad\qquad \bar{q} \in \{\bar{d},\bar{s},\bar{b}\}. \tag{28}$$

The expressions for $\tilde{f}$ read

$$\tilde{f}_{bu}^{(11)} = -2P_{qq}^{(0)} \otimes \tilde{f}_{qq}^{(0)}, \tag{29}$$

$$\tilde{f}_{b\bar{d}}^{(11)} = -2P_{qq}^{(0)} \otimes \tilde{f}_{q\bar{q}}^{(0)}, \tag{30}$$

$$\tilde{f}_{gu}^{(11)} = -P_{qg}^{(0)} \otimes \tilde{f}_{qq}^{(0)}, \tag{31}$$

$$\tilde{f}_{g\bar{d}}^{(11)} = -P_{qg}^{(0)} \otimes \tilde{f}_{q\bar{q}}^{(0)}, \tag{32}$$

$$\tilde{f}_{gb}^{(11)} = \tilde{f}_{gu}^{(11)} + \tilde{f}_{g\bar{d}}^{(11)}. \tag{33}$$

In case of associated production of a W boson and a top quark, the dependence on the CKM matrix can be written in the following way:

$$f_{gq}^{(i)} = \tilde{f}_{gb}^{(i)} \left|V_{tq}\right|^2, \qquad\qquad q \in \{d,s,b\}, i \in \{0, 10, 11\}, \tag{34}$$

$$f_{\mathrm{qq}}^{(j)} = 2\tilde{f}_{\mathrm{bu}}^{(j)} \left|V_{\mathrm{tq}}\right|^2, \qquad \mathrm{q} \in \{\mathrm{d,s,b}\}, \, j \in \{10,11\}, \tag{35}$$

$$f_{\mathrm{q_1 q_2}}^{(j)} = \tilde{f}_{\mathrm{bu}}^{(j)} \left|V_{\mathrm{tq_2}}\right|^2, \qquad \mathrm{q_1} \in \{\mathrm{u,d,c,s,b,\bar{u},\bar{d},\bar{c},\bar{s},\bar{b}}\}, \, \mathrm{q_2} \in \{\mathrm{d,s,b}\}, \, q_1 \neq q_2, \tag{36}$$

$$f_{\mathrm{gg}}^{(j)} = \tilde{f}_{\mathrm{gg}}^{(j)} \, \Sigma_{\mathrm{t}}. \tag{37}$$

The scale-dependent terms $\tilde{f}$ for the associated production are given by

$$\tilde{f}_{\mathrm{gb}}^{(11)} = \left(\beta_0 - P_{\mathrm{qq}}^{(0)} - P_{\mathrm{gg}}^{(0)}\right) \otimes \tilde{f}_{\mathrm{gq}}^{(0)}, \tag{38}$$

$$\tilde{f}_{\mathrm{gg}}^{(11)} = -2 P_{\mathrm{qg}}^{(0)} \otimes \tilde{f}_{\mathrm{gq}}^{(0)}, \tag{39}$$

$$\tilde{f}_{\mathrm{bu}}^{(11)} = -P_{\mathrm{gq}}^{(0)} \otimes \tilde{f}_{\mathrm{gq}}^{(0)}. \tag{40}$$

The functions $\tilde{f}^{(21)}$ and $\tilde{f}^{(22)}$ which correspond to each $\tilde{f}^{(20)}$ function in the NNLO case are collected in App. A.

2.3 Validation

In Tab. 1, all parameter settings used by the HATHOR program are listed. Some of the values are fixed and cannot be changed by the user. Most of the SM parameters as well as the PDF sets, however, can be varied as described in Sec. 3.

The extension of the HATHOR program to single top-quark production has been validated extensively for various parameter combinations. The numerical implementation of the analytic results in LO was checked with MCFM. No significant deviation was found. The same was done with the numerical computations in NLO. An example is shown in Fig. 3. Here, the relative deviation of the HATHOR results from the corresponding MCFM values for t-channel, s-channel and associated Wt production in pp collisions are shown as function of the top-quark mass. The mass dependence is of interest since its computation with HATHOR requires mass-dependent parameterisations of the partonic cross sections and a proper interpolation. As can be seen from Fig. 3, the deviations are well below 1‰ for the whole mass range. In the vicinity of the measured top-quark mass, the deviations are in most cases smaller than 0.5‰. Very similar results are observed for different centre-of-mass energies and other parameter settings.

3 HATHOR for single top-quark production

This paper marks the release of the 2.0 version of the HATHOR program, which is available for download at `http://www.physik.hu-berlin.de/pep/tools`. The installation of the package has changed with the new release compared to the previous versions. Detailed instructions how to install HATHOR can be found in a release note distributed together with the library.

Cross sections for top-quark pair production are evaluated in the same way as before by using the `Hathor` class, as described in [44, Sec. 4]. For inclusive single top-quark production, the new classes `HathorSgTopT`, `HathorSgTopS` and `HathorSgTopWt` for the three production channels are introduced. These classes and the `Hathor` class are derived from a common base class and thus provide the same methods for the calculation. Additionally, the following new common methods are implemented in the new classes for single top-quark production:

11
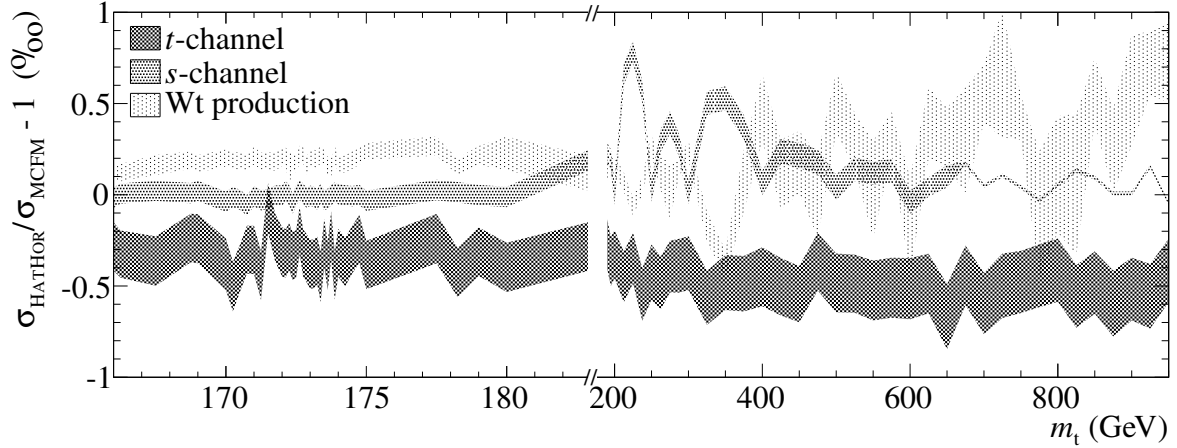
Figure 3: Cross sections for single top-quark production calculated with HATHOR for pp scattering at $\sqrt{s} = 14\,\text{TeV}$, compared with the corresponding MCFM results. For each production mode the relative deviation between both programs is shown. The width of the uncertainty bands indicates the statistical integration error of MCFM. The interesting area around the actual top-quark mass is enlarged on the left side of the figure.

void getCkmMatrix(double ckm[3][3])

This method can be used to determine the CKM matrix currently used by the HATHOR library. The values are copied into the array provided as the argument.

void setCkmMatrix(const double ckm[3][3])

This method allows to modify the CKM matrix. The default values are set according to the recent PDG world averages [51]. To change the settings, a 3×3 matrix with elements of type `double` representing the magnitudes of the CKM matrix elements has to be passed to this method. HATHOR does not check whether the provided matrix is unitary.

If only one entry of the CKM matrix needs to be changed, a call of the `getCkmMatrix` method may be useful:

```
Lhapdf pdf("CT10nlo");
HathorSgTopT hathor(pdf);
double ckm[3][3];
hathor.getCkmMatrix(ckm);
ckm[3][3]=1.;
hathor.setCkmMatrix(ckm);
```

PrintCkmMatrix()

This method prints the CKM matrix elements to the standard output.

setParticle(PARTICLE particle)

This method allows the user to choose the charge of the top-quarks to be produced. The three possible choices are defined as constants: `TOPQUARK`, `ANTITOPQUARK` or `BOTH`. The latter op-

tion evaluates the inclusive cross section for single top-quark and anti-quark production. By default, the cross section for single top-quark production is calculated.

The perturbative order of the cross section predictions can be selected using the method `setScheme` as in the $t\bar{t}$ case:

`LO`
This option enables the leading order contribution, which is derived from analytic results for the partonic cross sections implemented in HATHOR.

`NLO`
This option enables the next-to-leading order contribution, whose partonic cross sections have been sampled from MCFM. The scale-dependent terms are calculated using the results presented in the previous section. To obtain the full total cross section in NLO the user has to combine this option with the LO one.

The inclusion of the calculations into another program is demonstrated as an example in the `demo_sgtop.cxx` file . It makes use of all features provided by HATHOR. Another example is given in App. D. In addition, we provide a graphical user interface to the library, which may be useful if only a few reference cross sections are required.

When publishing results obtained with the HATHOR program please quote the references of the underlying calculations. At next-to-leading order this is [9] for t-channel and s-channel production and [18] for associated Wt production.

4 Results

A key feature of the HATHOR program is the possibility to vary certain model parameters which allows fast computations of the total cross section dependencies on such parameters. In this section, several examples for such studies are presented.

Cross sections in higher orders
Figure 4 shows the cross section for single top-quark t-channel production as function of the centre-of-mass-energy in pp and p$\bar{\text{p}}$ scattering. Leading order and NLO calculations are presented. The uncertainty bands indicate the uncertainty estimated by the combined variation of μ_R and μ_F by factors between $1/2$ and 2. More detailed studies of the scale dependence of the cross sections and their respective uncertainties are given in the next paragraph. For comparison, also the latest measurements from the CDF and the D∅ experiments as well as from ATLAS and CMS are shown in Fig. 4. The cross sections for the s-channel and associated Wt production are depicted in Fig. 11 in the appendix. On a standard 2.4 GHz Xeon CPU, the entire calculations for Fig. 4 were performed in about 15 minutes with the HATHOR program.

Renormalisation and factorisation scale (in)dependence
The scale dependence of the cross section for the different orders is given by Eqs. (14–15) which allow fast computations for any given pair of μ_R and μ_F. As an example, we show in Fig. 5 cross section contours obtained from an independent variation of μ_F and μ_R. Since $f_{ij}^{(20)}$ is not yet fully known, we include only the scale dependence at NLO accuracy (i.e. Eq. (15)) in
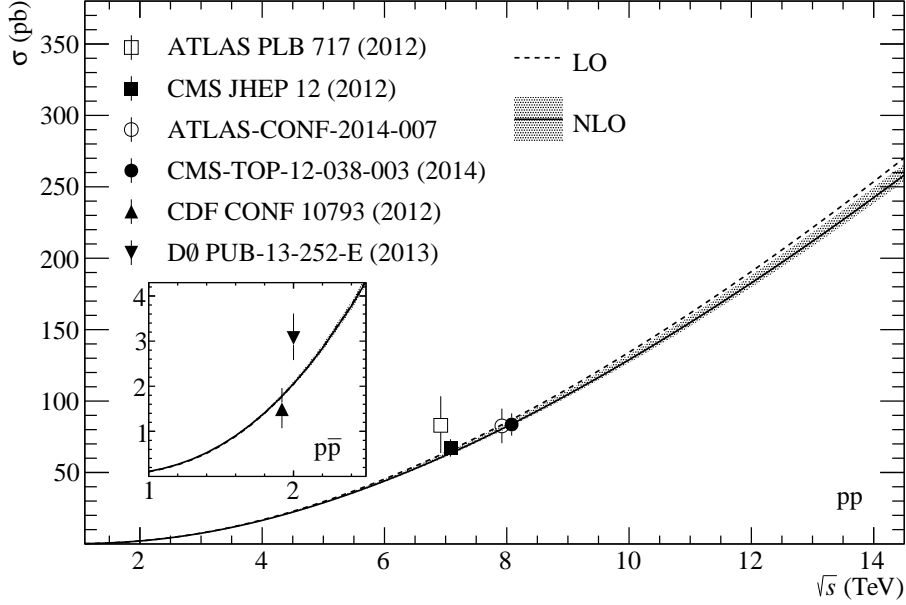
Figure 4: LO and NLO cross section for *t*-channel single top-quark production calculated with the HATHOR program using CT10nlo as PDF set. The uncertainty band shown for NLO indicates the scale uncertainty. The latest measurements from the LHC [35, 36, 53, 54] and the Tevatron [55, 56] are shown for comparison.

the analysis.[2] In case of *t* and *s*-channel production, one observes that for a reasonable change of the scales the cross section varies by less than five per cent. In the *s*-channel the μ_F and μ_R dependencies are anti-correlated. Using a naive variation $m_t/2 < \mu < 2m_t$ with $\mu = \mu_F = \mu_R$ thus underestimates the scale uncertainty. In the Wt-channel the residual scale uncertainty is slightly larger. Again, a variation along the diagonal in the $\mu_F - \mu_R$ plane underestimates the uncertainty.

Top-quark mass
The HATHOR program also allows to vary the pole mass of the top quark, m_t, over a wide range. This is shown in Fig. 6 in NLO for the case of pp scattering at 14 TeV. In the figure, the mass range around the measured top-quark mass is shown together with a mass range extended up to 1 TeV which might be of interest for certain heavy quark searches.

Following up on [24], the cross section dependence on the top-quark mass can be approximated to a precision of 1 % by

$$\sigma(m_t) = \sigma(\bar{m}_t) \left[1 + A \times \left(\frac{m_t - \bar{m}_t}{\bar{m}_t} \right) + B \times \left(\frac{m_t - \bar{m}_t}{\bar{m}_t} \right)^2 \right], \tag{41}$$

where $\bar{m}_t$ is chosen to be 173.5 GeV [51]. The coefficients for all three production channels are given in Tab. 3 in App. C for centre-of-mass energies at 8 TeV and 14 TeV, as well as for four different PDF sets. The parameter *A* relates the relative change of the cross section with

---

[2]Using an educated guess for the yet uncalculated $f_{ij}^{(20)}$ one may use Eq. (16) to estimate the possible improvements once the full NNLO calculation is available.
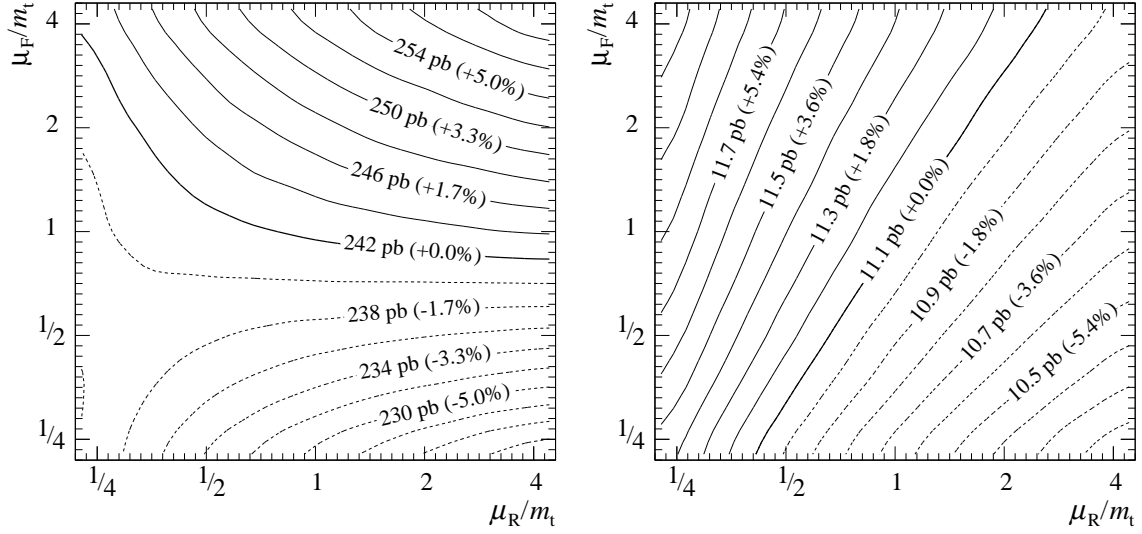
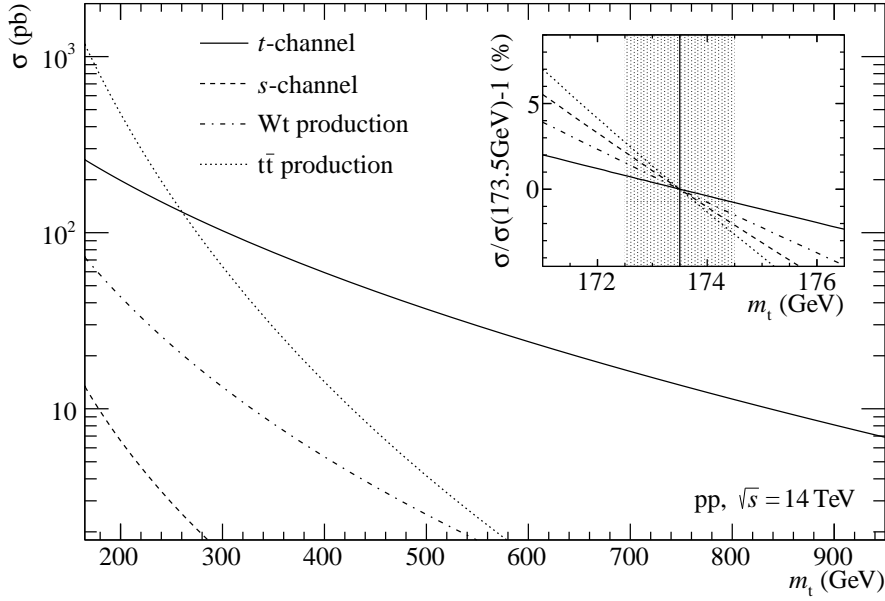**(a)** *t*-channel production

(b) *s*-channel production
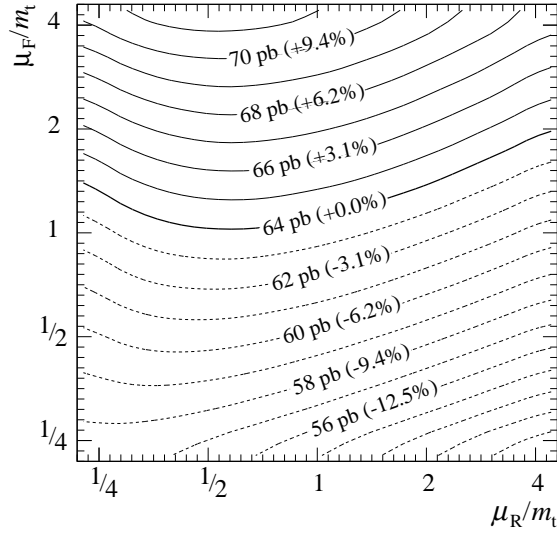
(c) Associated Wt production

Figure 5: Two-dimensional cross section dependence on the renormalisation scale, μ_R, and the factorisation scale, μ_F, of the three single top-quark production channels in pp collisions at $\sqrt{s} = 14\,\text{TeV}$ in NLO using CT10nlo. The fat contour line in each figure indicates the reference cross section value for $\mu_R = \mu_F = m_t$. Contour lines for cross sections below (above) the reference cross section are drawn as dashed (solid thin) lines.

the relative change in m_t close to $\bar{m}_t$. For the three modes of single top-quark production (not $\bar{t}$), the results for a centre-of-mass energy of $8\,\text{TeV}$ are

$$\frac{\Delta\sigma_t}{\sigma_t} = -1.6 \times \frac{\Delta m_t}{m_t}, \quad \frac{\Delta\sigma_s}{\sigma_s} = -3.9 \times \frac{\Delta m_t}{m_t}, \quad \frac{\Delta\sigma_{Wt}}{\sigma_{Wt}} = -3.1 \times \frac{\Delta m_t}{m_t}, \quad (42)$$

15

Figure 6: Top-quark production cross sections for different top-quark masses. The single top-quark production is calculated in NLO with CT10nlo, whereas top-quark pair production employs NNLO with CT10nnlo. The in-set shows the relative change of the cross section around the actual top-quark mass.

with slightly smaller slopes for an energy of 14 TeV,

$$\frac{\Delta \sigma_t}{\sigma_t} = -1.4 \times \frac{\Delta m_{\mathrm{t}}}{m_{\mathrm{t}}}, \quad \frac{\Delta \sigma_s}{\sigma_s} = -3.7 \times \frac{\Delta m_{\mathrm{t}}}{m_{\mathrm{t}}}, \quad \frac{\Delta \sigma_{\mathrm{Wt}}}{\sigma_{\mathrm{Wt}}} = -2.7 \times \frac{\Delta m_{\mathrm{t}}}{m_{\mathrm{t}}}. \tag{43}$$

The parameter *A* hence determines the experimental sensitivity for extracting the top-quark mass from a measurement of single top-quark production cross sections. The production in the *s*-channel exhibits the strongest top-quark mass dependence, in particular for lower centre-of-mass energies (cf. Tab. 3). In Fig. 7, top-quark masses extracted in this way from recent measurements are presented. The results are given using the relation between the mass and the cross section at NLO accuracy. Evidently, the uncertainty of the extracted top-quark masses is large as a consequence of the weak sensitivity. Within the uncertainties, the results are consistent with the world average.

Strong coupling constant

The strong coupling constant, α_{s}, enters the computation through the matrix elements and through the parton distribution functions. Since the parton distribution functions and α_{s} are highly correlated when determined in global fits, it is not sufficient for α_{s} uncertainty studies to change only α_{s}. For a precise estimate of the uncertainty, it is important to use PDF sets providing fits for different α_{s} values. In Fig. 8, we show as an example the dependence of the single top-quark *t*-channel cross section. The computation is performed at NLO accuracy at a centre-of-mass energy of 14 TeV for proton-proton scattering. The best fit values for each PDF set as well as the latest measurement for $\alpha_{\mathrm{s}}(m_{\mathrm{Z}}^2)$ are shown for comparison. As one would have naively expected, we observe to good approximation a linear dependence on α_{s}

16
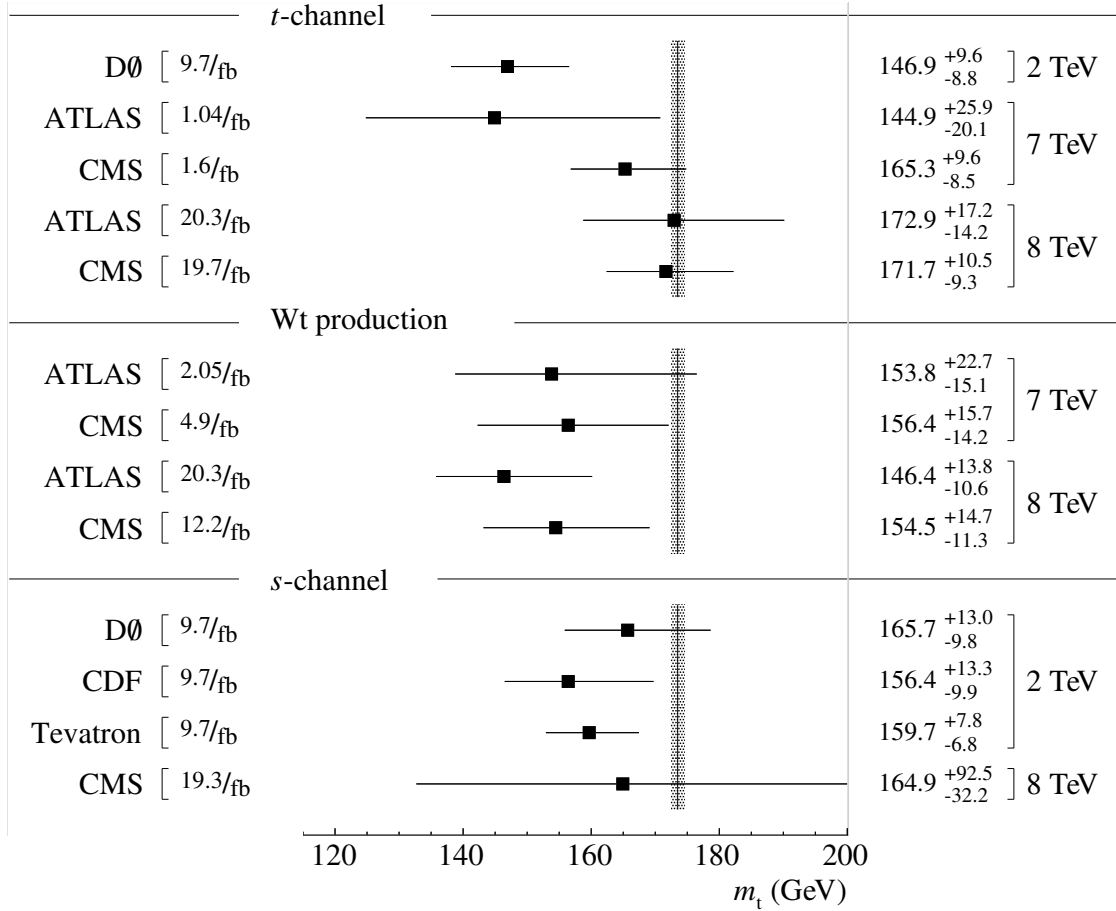
Figure 7: Overview of top-quark masses obtained from recent cross section measurements of single top-quark production. All masses are given with respect to the NLO prediction using CT10nlo. Their numerical values are listed on the right side of the figure. All numbers are in GeV. The vertical line denotes the current world average of the top-quark mass from measurements of $t\bar{t}$ production [51]; the shaded band indicates the uncertainty. The cross section values used here are taken from the measurements [35, 38, 53, 57] of the ATLAS collaboration, [58] of the CDF collaboration, [36, 37, 39, 40, 54] of the CMS collaboration and [56] of the DØ collaboration. The combined Tevatron measurement is taken from [42].

with a slope close to one. A one per cent uncertainty in α_s thus roughly translates to a one per cent uncertainty of the cross section. In addition, Fig. 8 shows that the ABM11 PDF [59] leads to significantly larger predictions for the cross sections. The corresponding plots for the s-channel and associated Wt production are given in Figs. 12a, 12b in App. B.

PDF uncertainties
Examples for the uncertainty related to our imperfect knowledge of the parton distribution functions are shown Fig. 9 for the three different channels contributing to single top-quark production. For the PDF sets we used ABM11 [59], CT10 [60], MSTW08 [61] and NNPDF23 [62]. The uncertainty bands include the uncertainties from the PDF fits as well as the α_s dependence. The results are normalised to the cross sections calculated using CT10. The uncertainties for the individual PDF sets are typically at the level of ± 2.5 per cent at very low
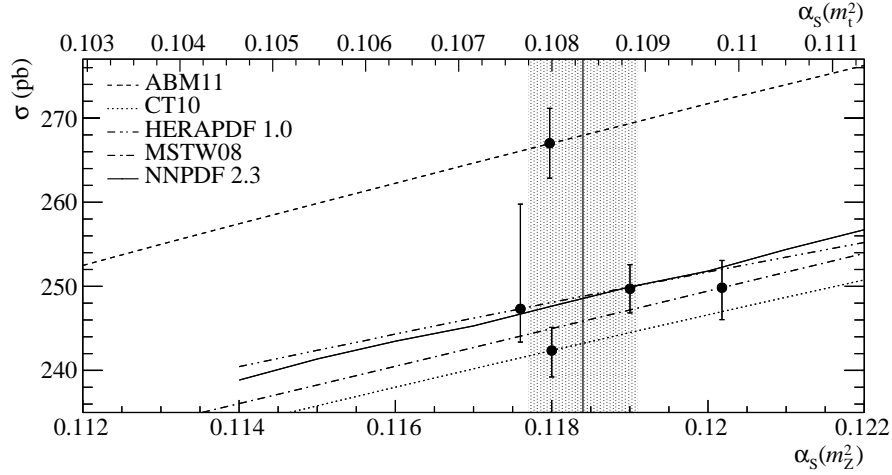
Figure 8: Single top-quark t-channel cross section in NLO for different values of α_s, computed for different NLO PDFs at $\sqrt{s} = 14\,\text{TeV}$ in pp scattering. For each PDF set, the best fit value and the corresponding full PDF uncertainty is indicated by the black marker and the error bar. The α_s values are given with respect to the mass of the Z boson (lower abscissa) and the mass of the top quark (upper abscissa). The vertical line and the shaded box represent the latest world average value of α_s and its uncertainty at the Z pole [51].

energies and ± 1 per cent at high energies in case of the s and t-channels. In case of associated Wt production the uncertainties are significantly larger. Comparing different PDF sets, the CT10 predictions are slightly below the predictions obtained using MSTW08 and NNPDF23. ABM11 on the other hand leads to significantly larger cross sections at high energies for the t-channel, while for the Wt production the cross section is suppressed at low energies compared to other PDFs. Within the uncertainty bands the results are, however, marginally consistent.

Table 2 provides a breakdown of the uncertainties for several PDF sets. The contributions from the different sources of uncertainties are listed here for the case of t-channel production in pp collisions at $14\,\text{TeV}$.

| PDF Set	Cross section	PDF uncert.	α_s uncert.	PDF+α_s uncert.	Scale uncert.
ABM11	267.0 pb	$\pm 1.3\%$	$\pm 0.8\%$	$\pm 1.6\%$	$^{+2.8\%}_{-1.6\%}$
CT10	242.4 pb	$^{+0.9\%}_{-1.1\%}$	$^{+0.7\%}_{-0.8\%}$	$^{+1.1\%}_{-1.3\%}$	$^{+3.0\%}_{-1.7\%}$
HERAPDF 1.0	247.3 pb	$^{+5.0\%}_{-1.3\%}$	$\pm 0.9\%$	$^{+5.0\%}_{-1.6\%}$	$^{+3.3\%}_{-1.7\%}$
MSTW 2008	249.8 pb	$\pm 0.6\%$	$^{+1.2\%}_{-1.4\%}$	$^{+1.3\%}_{-1.5\%}$	$^{+3.0\%}_{-1.6\%}$
NNPDF 2.3	249.6 pb	$\pm 0.5\%$	$\pm 1.1\%$	$\pm 1.2\%$	$^{+3.2\%}_{-1.8\%}$

Table 2: Sources of uncertainties for single top-quark production cross sections at NLO for the t-channel in pp collisions with $\sqrt{s} = 14\,\text{TeV}$ for various NLO PDF sets including the HERAPDF [64].
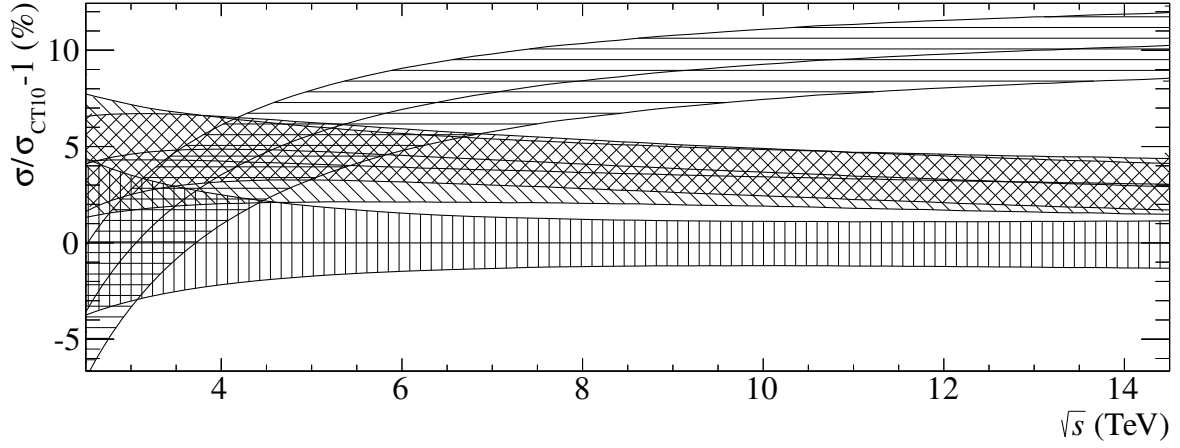
(a) *t*-channel production
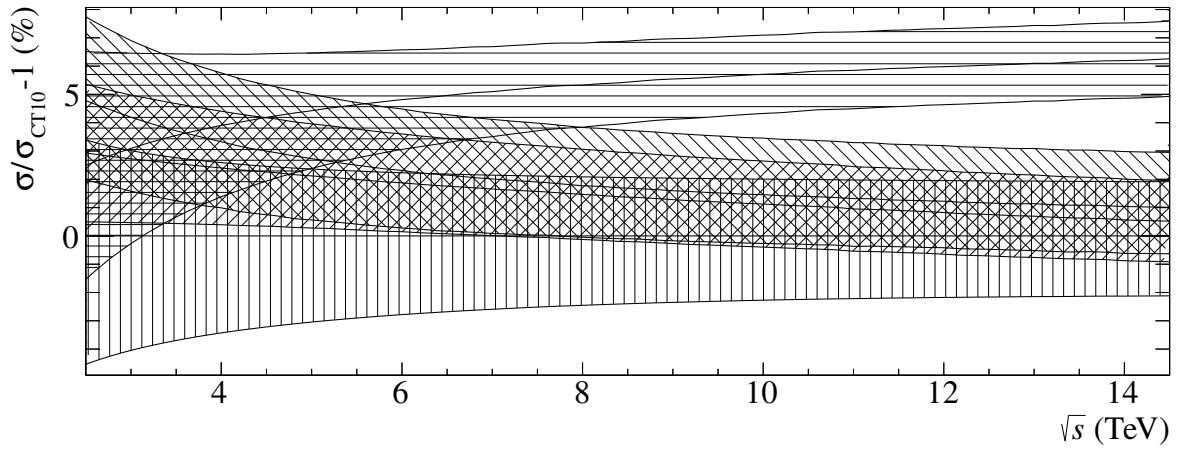
(b) *s*-channel production
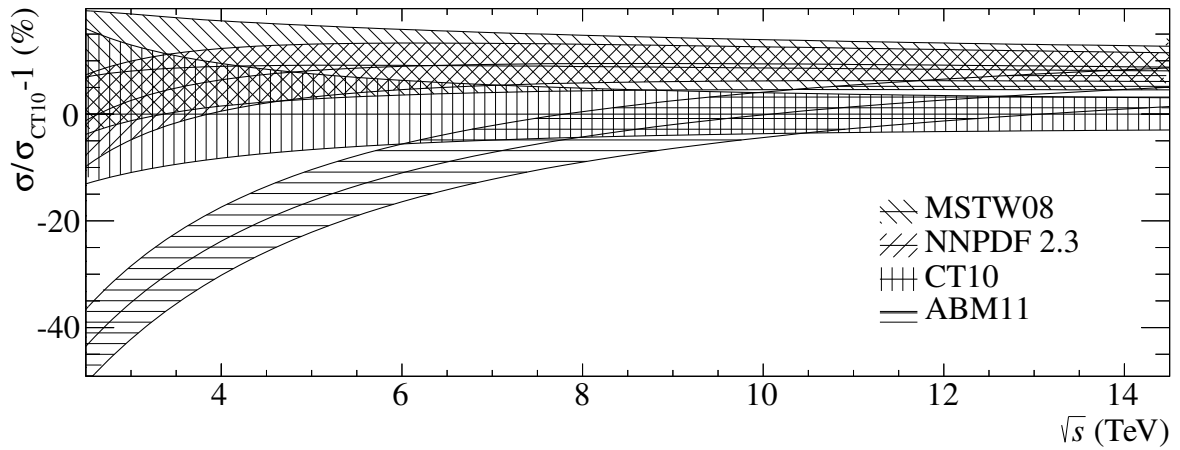
(c) Associated Wt production

Figure 9: PDF uncertainties for the predicted cross sections for single top-quark production in proton-proton scattering as function of the centre-of-mass energy, $\sqrt{s}$. The uncertainty bands are calculated according to [59] for ABM11, [60] for CT10, [61] for MSTW08 and [63] for NNPDF23 (all PDFs in NLO accuracy). All uncertainties are given with respect to CT10.

5 Summary

The extension of the HATHOR cross section calculator for the production of single top-quarks has been presented. The new part comprises a fast computation of all three production channels, the *t*-channel, the *s*-channel and the associated Wt production, in LO and NLO of QCD. Despite the small amount of computing time needed, the results agree within less than 1‰ with those from other programs. Moreover, the complete scale dependence for μ_R and μ_F of the cross sections is implemented for all orders up to NNLO and the corresponding equations are collected in this paper.

Besides the scales, the HATHOR program allows to vary several model parameters and the PDFs. This can be used to establish thorough systematic studies of the total cross section in a fast and efficient manner. Several examples were presented here, mostly for proton-proton scattering at the LHC. Among these are cross section calculations in different orders and the dependence on renormalisation and factorisation scales. The dependence on the mass of the top quark was studied in some detail and estimates of the top-quark mass from single top-quark production using the latest cross section measurements were given. Furthermore, the impact of the strong coupling constant, α_s, and the parton distribution functions on the cross section uncertainty has been discussed.

A Scaling functions in NNLO

Using

$$P_{q_i q_j} = \delta_{ij} P_{qq}^V + P_{qq}^S, \tag{44}$$

$$P_{q_i \bar{q}_j} = \delta_{ij} P_{q\bar{q}}^V + P_{q\bar{q}}^S, \tag{45}$$

the scale dependent terms for *s*-channel read ($i \in \{20, 21, 22\}$):

$$f_{qq'}^{(i)} = \tilde{f}_{u\bar{d}}^{(i)} \left| V_{qq'} \right|^2 \Sigma_t + \tilde{f}_{uc}^{(i)} \left(\Sigma_q + \Sigma_{q'} \right) \Sigma_t \qquad q \in \{u, c\} \quad , q' \in \{\bar{b}, \bar{s}, \bar{d}\},$$

$$f_{qq'}^{(i)} = \tilde{f}_{uc}^{(i)} \Sigma_q \Sigma_t + \tilde{f}_{ud}^{(i)} \left| V_{qq'} \right|^2 \Sigma_t \qquad qq' \in \{cb, cd, cs, ub, ud, us, \bar{b}u, \bar{b}c, \bar{s}u, \bar{s}c, \bar{d}u, \bar{d}c\}$$

$$f_{qq'}^{(i)} = \tilde{f}_{uc}^{(i)} \left(\Sigma_q + \Sigma_{q'} \right) \Sigma_t \qquad qq' \in \{uc, uu, cc, \bar{d}\bar{d}, \bar{s}\bar{s}, \bar{b}\bar{b}, \bar{d}\bar{s}, \bar{d}\bar{b}, \bar{s}\bar{b}\}$$

$$f_{qq'}^{(i)} = \tilde{f}_{uc}^{(i)} \Sigma_q \Sigma_t \qquad qq' \in \{u\bar{u}, u\bar{c}, c\bar{u}, c\bar{c}, \bar{b}b, \bar{b}d, \bar{b}s, \bar{s}b, \bar{s}d, \bar{s}s, \bar{d}b, \bar{d}d, \bar{d}s\}$$

$$f_{gq}^{(i)} = \tilde{f}_{gu}^{(i)} \Sigma_q \Sigma_t \qquad q \in \{\bar{b}, \bar{d}, \bar{s}, c, u\}$$

$$f_{gg}^{(i)} = \tilde{f}_{gg}^{(i)} \left(\Sigma_u + \Sigma_c \right) \Sigma_t$$

with

$$\tilde{f}_{u\bar{d}}^{(21)} = -2\,P_{qq}^{V(1)} \otimes \tilde{f}_{u\bar{d}}^{(0)} + \left(\beta_0 - 2P_{qq}^{(0)}\right) \otimes \tilde{f}_{u\bar{d}}^{(10)},$$

$$\tilde{f}_{u\bar{d}}^{(22)} = \left(-\beta_0 P_{qq}^{(0)} + 2P_{qq}^{(0)} \otimes P_{qq}^{(0)}\right) \otimes \tilde{f}_{u\bar{d}}^{(0)},$$

$$\tilde{f}_{gu}^{(21)} = -P_{qg}^{(1)} \otimes \tilde{f}_{u\bar{d}}^{(0)} - P_{qg}^{(0)} \otimes \tilde{f}_{u\bar{d}}^{(10)} + \left(\beta_0 - P_{qq}^{(0)} - P_{gg}^{(0)}\right) \otimes \tilde{f}_{gu}^{(10)},$$

$$\tilde{f}_{gu}^{(22)} = \frac{1}{2}\left(3P_{qq}^{(0)} \otimes P_{qg}^{(0)} - \beta_0 P_{qg}^{(0)} + P_{qg}^{(0)} \otimes P_{gg}^{(0)}\right) \otimes \tilde{f}_{u\bar{d}}^{(0)},$$

$$\tilde{f}_{gg}^{(21)} = -4\,P_{qg}^{(0)} \otimes \tilde{f}_{gu}^{(10)},$$

$$\tilde{f}_{gg}^{(22)} = 2\,P_{qg}^{(0)} \otimes P_{qg}^{(0)} \otimes \tilde{f}_{u\bar{d}}^{(0)},$$

$$\tilde{f}_{uc}^{(21)} = -P_{qq}^{S(1)} \otimes \tilde{f}_{u\bar{d}}^{(0)} - P_{gq}^{(0)} \otimes \tilde{f}_{gu}^{(10)},$$

$$\tilde{f}_{uc}^{(22)} = \frac{1}{2}\,P_{qg}^{(0)} \otimes P_{gq}^{(0)} \otimes \tilde{f}_{u\bar{d}}^{(0)},$$

$$\tilde{f}_{ud}^{(21)} = -P_{q\bar{q}}^{V(1)} \otimes \tilde{f}_{u\bar{d}}^{(0)},$$

$$\tilde{f}_{ud}^{(22)} = 0.$$

t-channel:

$$f_{qq'}^{(i)} = \tilde{f}_{bu}^{(i)}\,\Sigma_q\,|V_{tq'}|^2 + \tilde{f}_{uc}^{(i)}\,\Sigma_q\Sigma_t + \tilde{f}_{bd}^{(i)}\,(\Sigma_u + \Sigma_c)\,|V_{tq'}|^2 \qquad q \in \{c,u\}, q' \in \{d,s,b\}$$

$$f_{qq'}^{(i)} = \tilde{f}_{b\bar{d}}^{(i)}\,\Sigma_q\,|V_{tq'}|^2 + \tilde{f}_{\bar{d}u}^{(i)}\,\Sigma_q\Sigma_t + \tilde{f}_{bd}^{(i)}\,(\Sigma_u + \Sigma_c)\,|V_{tq'}|^2 \qquad q \in \{\bar{d},\bar{s},\bar{b}\}, q' \in \{d,s,b\}$$

$$f_{qq'}^{(i)} = \tilde{f}_{b\bar{u}}^{(i)}\,\Sigma_q\,|V_{tq'}|^2 + \tilde{f}_{bd}^{(i)}\,(\Sigma_u + \Sigma_c)\,|V_{tq'}|^2 \qquad q \in \{\bar{c},\bar{u}\}, q' \in \{d,s,b\}$$

$$f_{qq'}^{(i)} = \tilde{f}_{b\bar{u}}^{(i)}\,\Sigma_q\,|V_{tq'}|^2 + \tilde{f}_{uc}^{(i)}\,\Sigma_q\Sigma_t + \tilde{f}_{\bar{d}u}^{(i)}\,\Sigma_{q'}\Sigma_t \qquad q \in \{c,u\}, q' \in \{\bar{d},\bar{s},\bar{b}\}$$

$$f_{qq'}^{(i)} = \tilde{f}_{\bar{d}\bar{b}}^{(i)}\,(\Sigma_q\,|V_{tq'}|^2 + \Sigma_{q'}\,|V_{tq}|^2) + \tilde{f}_{bd}^{(i)}\,(\Sigma_u + \Sigma_c)(|V_{tq'}|^2 + |V_{tq}|^2) \qquad q \in \{d,s,b\}, q' \in \{d,s,b\}$$

$$f_{qq'}^{(i)} = \tilde{f}_{\bar{d}u}^{(i)}\,(\Sigma_q + \Sigma_{q'})\Sigma_t + \tilde{f}_{\bar{d}\bar{b}}^{(i)}\,(\Sigma_q\,|V_{tq'}|^2 + \Sigma_{q'}\,|V_{tq}|^2) \qquad q \in \{\bar{d},\bar{s},\bar{b}\}, q' \in \{\bar{d},\bar{s},\bar{b}\}$$

$$f_{qq'}^{(i)} = \tilde{f}_{\bar{d}\bar{b}}^{(i)}\,\Sigma_q\Sigma_t \qquad q \in \{\bar{d},\bar{s},\bar{b}\}, q' \in \{\bar{u},\bar{c}\}$$

$$f_{qq'}^{(i)} = \tilde{f}_{uc}^{(i)}\,\Sigma_q\Sigma_t \qquad q \in \{u,c\}, q' \in \{\bar{u},\bar{c}\}$$

$$f_{qq'}^{(i)} = \tilde{f}_{uc}^{(i)}\,(\Sigma_q + \Sigma_{q'})\Sigma_t \qquad q \in \{u,c\}, q' \in \{u,c\}$$

$$f_{gq}^{(i)} = \tilde{f}_{gb}^{(i)}\,(\Sigma_u + \Sigma_c)\,|V_{tq}|^2 \qquad q \in \{b,d,s\}$$

$$f_{gq}^{(i)} = \tilde{f}_{g\bar{b}}^{(i)}\,\Sigma_{\bar{q}}\Sigma_t \qquad q \in \{\bar{b},\bar{d},\bar{s}\}$$

$$f_{gq}^{(i)} = \tilde{f}_{gu}^{(i)}\,\Sigma_q\Sigma_t \qquad q \in \{c,u\}$$

$$f_{gg}^{(i)} = \tilde{f}_{gg}^{(i)}\,(\Sigma_u + \Sigma_c)\Sigma_t$$

with

$$\tilde{f}_{bu}^{(21)} = -2\,P_{qq}^{V(1)} \otimes \tilde{f}_{bu}^{(0)} + \left(\beta_0 - 2P_{qq}^{(0)}\right) \otimes \tilde{f}_{bu}^{(10)},$$

$$\tilde{f}_{bu}^{(22)} = \left(-\beta_0 P_{qq}^{(0)} + 2P_{qq}^{(0)} \otimes P_{qq}^{(0)}\right) \otimes \tilde{f}_{bu}^{(0)},$$

$$\tilde{f}_{b\bar{d}}^{(21)} = -2P_{qq}^{V(1)} \otimes \tilde{f}_{b\bar{d}}^{(0)} + \left(\beta_0 - 2P_{qq}^{(0)}\right) \otimes \tilde{f}_{b\bar{d}}^{(10)},$$

$$\tilde{f}_{b\bar{d}}^{(22)} = \left(-\beta_0 P_{qq}^{(0)} + 2P_{qq}^{(0)} \otimes P_{qq}^{(0)}\right) \otimes \tilde{f}_{b\bar{d}}^{(0)},$$

$$\tilde{f}_{gu}^{(21)} = -P_{qg}^{(1)} \otimes \tilde{f}_{bu}^{(0)} - P_{qg}^{(0)} \otimes \tilde{f}_{bu}^{(10)} + \left(\beta_0 - P_{qq}^{(0)} - P_{gg}^{(0)}\right) \otimes \tilde{f}_{gu}^{(10)}$$

$$\tilde{f}_{gu}^{(22)} = \frac{1}{2}\left(3P_{qq}^{(0)} \otimes P_{qg}^{(0)} - \beta_0 P_{qg}^{(0)} + P_{qg}^{(0)} \otimes P_{gg}^{(0)}\right) \otimes \tilde{f}_{bu}^{(0)},$$

$$\tilde{f}_{g\bar{d}}^{(21)} = -P_{qg}^{(1)} \otimes \tilde{f}_{b\bar{d}}^{(0)} - P_{qg}^{(0)} \otimes \tilde{f}_{b\bar{d}}^{(10)} + \left(\beta_0 - P_{qq}^{(0)} - P_{gg}^{(0)}\right) \otimes \tilde{f}_{g\bar{u}}^{(10)}$$

$$\tilde{f}_{g\bar{d}}^{(22)} = \frac{1}{2}\left(3P_{qq}^{(0)} \otimes P_{qg}^{(0)} - \beta_0 P_{qg}^{(0)} + P_{qg}^{(0)} \otimes P_{gg}^{(0)}\right) \otimes \tilde{f}_{b\bar{d}}^{(0)},$$

$$\tilde{f}_{gb}^{(21)} = -P_{qg}^{(1)} \otimes \tilde{f}_{bu}^{(0)} - P_{qg}^{(0)} \otimes \tilde{f}_{bu}^{(10)} - P_{qg}^{(1)} \otimes \tilde{f}_{b\bar{d}}^{(0)} - P_{qg}^{(0)} \otimes \tilde{f}_{b\bar{d}}^{(10)}$$
$$+ \left(\beta_0 - P_{qq}^{(0)} - P_{gg}^{(0)}\right) \otimes \tilde{f}_{gb}^{(10)}$$

$$\tilde{f}_{gb}^{(22)} = \tilde{f}_{gu}^{(22)} + \tilde{f}_{g\bar{d}}^{(22)},$$

$$\tilde{f}_{gg}^{(21)} = -2P_{qg}^{(0)} \otimes \tilde{f}_{gu}^{(10)} - 2P_{qg}^{(0)} \otimes \tilde{f}_{gb}^{(10)} - 2P_{qg}^{(0)} \otimes \tilde{f}_{g\bar{d}}^{(10)},$$

$$\tilde{f}_{gg}^{(22)} = 2P_{qg}^{(0)} \otimes P_{qg}^{(0)} \otimes \tilde{f}_{bu}^{(0)} + 2P_{qg}^{(0)} \otimes P_{qg}^{(0)} \otimes \tilde{f}_{b\bar{d}}^{(0)},$$

$$\tilde{f}_{uc}^{(21)} = -P_{qq}^{S(1)} \otimes \tilde{f}_{bu}^{(0)} - P_{gq}^{(0)} \otimes \tilde{f}_{gu}^{(10)},$$

$$\tilde{f}_{uc}^{(22)} = \frac{1}{2}P_{qg}^{(0)} \otimes P_{gq}^{(0)} \otimes \tilde{f}_{bu}^{(0)},$$

$$\tilde{f}_{\bar{d}\bar{u}}^{(21)} = -P_{qq}^{S(1)} \otimes \tilde{f}_{b\bar{d}}^{(0)} - P_{gq}^{(0)} \otimes \tilde{f}_{g\bar{d}}^{(10)},$$

$$\tilde{f}_{\bar{d}\bar{u}}^{(22)} = \frac{1}{2}P_{qg}^{(0)} \otimes P_{gq}^{(0)} \otimes \tilde{f}_{b\bar{d}}^{(0)},$$

$$\tilde{f}_{bd}^{(21)} = -P_{qq}^{S(1)} \otimes \tilde{f}_{bu}^{(0)} - P_{qq}^{S(1)} \otimes \tilde{f}_{b\bar{d}}^{(0)} - P_{gq}^{(0)} \otimes \tilde{f}_{gb}^{(10)},$$

$$\tilde{f}_{bd}^{(22)} = \frac{1}{2}\left(P_{qg}^{(0)} \otimes P_{gq}^{(0)} \otimes \tilde{f}_{bu}^{(0)} + P_{qg}^{(0)} \otimes P_{gq}^{(0)} \otimes \tilde{f}_{b\bar{d}}^{(0)}\right),$$

$$\tilde{f}_{\bar{d}\bar{b}}^{(21)} = -P_{q\bar{q}}^{V(1)} \otimes \tilde{f}_{b\bar{d}}^{(0)},$$

$$\tilde{f}_{b\bar{u}}^{(21)} = -P_{q\bar{q}}^{V(1)} \otimes \tilde{f}_{bu}^{(0)},$$

$$\tilde{f}_{\bar{d}\bar{b}}^{(22)} = \tilde{f}_{b\bar{u}}^{(22)} = 0.$$

Associated Wt production, $i \in \{20, 21, 22\}, \kappa = 0$ for all partonic channels. If bb and $\bar{b}b$ are not included, $f_{gb}^{(i)}$ and $f_{g\bar{b}}^{(i)}$ change ($\kappa = 1$):

$$f_{gq}^{(i)} = \tilde{f}_{gb}^{(i)} |V_{tq}|^2 + \tilde{f}_{gu}^{(i)} \Sigma_t \qquad q \in \{b, d, s\}$$

$$f_{g\bar{q}}^{(i)} = \tilde{f}_{g\bar{b}}^{(i)} |V_{t\bar{q}}|^2 + \tilde{f}_{gu}^{(i)} \Sigma_t \qquad \bar{q} \in \{\bar{b}, \bar{d}, \bar{s}\}$$

$$f_{qq}^{(i)} = 2\tilde{f}_{bu}^{(i)} |V_{tq}|^2 \qquad q \in \{d, s, b\},$$

$$f_{qq'}^{(i)} = \tilde{f}_{bu}^{(i)} |V_{tq'}|^2 \qquad q \in \{\bar{b}, \bar{c}, \bar{s}, \bar{u}, \bar{d}, d, u, s, c, b\}, q' \in \{d, s, b\}, q \neq q'$$

$$f_{gq}^{(i)} = \tilde{f}_{gu}^{(i)} \Sigma_t \qquad q \in \{\bar{c}, \bar{u}, c, u\}$$

$$f_{\text{gg}}^{(i)} = \tilde{f}_{\text{gg}}^{(i)} \, \Sigma_{\text{t}}$$

with

$$\tilde{f}_{\text{gb}}^{(21)} = -(2\,n_{\text{f}} - 3\kappa) P_{\text{qg}}^{(0)} \otimes \tilde{f}_{\text{bu}}^{(10)} + \left(\beta_1 - P_{\text{gg}}^{(1)} - P_{\text{qq}}^{V(1)} \right) \otimes \tilde{f}_{\text{gb}}^{(0)}$$
$$+ \left(2\beta_0 - P_{\text{qq}}^{(0)} - P_{\text{gg}}^{(0)} \right) \otimes \tilde{f}_{\text{gb}}^{(10)} \, ,$$

$$\tilde{f}_{\text{gb}}^{(22)} = \left(\beta_0^2 - \frac{3}{2}\beta_0 P_{\text{qq}}^{(0)} + \frac{1}{2} P_{\text{qq}}^{(0)} \otimes P_{\text{qq}}^{(0)} + P_{\text{qq}}^{(0)} \otimes P_{\text{gg}}^{(0)} + \frac{1}{2}(2\,n_{\text{f}} - 3\kappa) P_{\text{qg}}^{(0)} \otimes P_{\text{gq}}^{(0)} \right.$$
$$\left. - \frac{3}{2}\beta_0 P_{\text{gg}}^{(0)} + \frac{1}{2} P_{\text{gg}}^{(0)} \otimes P_{\text{gg}}^{(0)} \right) \otimes \tilde{f}_{\text{gb}}^{(0)} \, ,$$

$$\tilde{f}_{\text{gg}}^{(21)} = -2 P_{\text{qg}}^{(1)} \otimes \tilde{f}_{\text{gb}}^{(0)} - 2 P_{\text{qg}}^{(0)} \otimes \tilde{f}_{\text{gb}}^{(10)} + 2 \left(\beta_0 - P_{\text{gg}}^{(0)} \right) \otimes \tilde{f}_{\text{gg}}^{(10)} \, ,$$

$$\tilde{f}_{\text{gg}}^{(22)} = \left(P_{\text{qq}}^{(0)} \otimes P_{\text{qg}}^{(0)} - 3\beta_0 P_{\text{qg}}^{(0)} + 3 P_{\text{qg}}^{(0)} \otimes P_{\text{gg}}^{(0)} \right) \otimes \tilde{f}_{\text{gb}}^{(0)} \, ,$$

$$\tilde{f}_{\text{bu}}^{(21)} = \left(2\beta_0 - 2 P_{\text{qq}}^{(0)} \right) \otimes \tilde{f}_{\text{bu}}^{(10)} - P_{\text{gq}}^{(1)} \otimes \tilde{f}_{\text{gb}}^{(0)} - P_{\text{gq}}^{(0)} \otimes \tilde{f}_{\text{gb}}^{(10)} \, ,$$

$$\tilde{f}_{\text{bu}}^{(22)} = \frac{1}{2} \left(3 P_{\text{qq}}^{(0)} \otimes P_{\text{gq}}^{(0)} - 3 \beta_0 P_{\text{gq}}^{(0)} + P_{\text{gq}}^{(0)} \otimes P_{\text{gg}}^{(0)} \right) \otimes \tilde{f}_{\text{gb}}^{(0)} \, ,$$

$$\tilde{f}_{\text{gu}}^{(21)} = -P_{\text{qg}}^{(0)} \otimes \tilde{f}_{\text{bu}}^{(10)} - P_{\text{qq}}^{S(1)} \otimes \tilde{f}_{\text{gb}}^{(0)} - P_{\text{gq}}^{(0)} \otimes \tilde{f}_{\text{gg}}^{(10)} \, ,$$

$$\tilde{f}_{\text{gu}}^{(22)} = \frac{3}{2} P_{\text{qg}}^{(0)} \otimes P_{\text{gq}}^{(0)} \otimes \tilde{f}_{\text{gb}}^{(0)} \, ,$$

$$\tilde{f}_{\text{g}\bar{\text{b}}}^{(21)} = -P_{\text{q}\bar{\text{q}}}^{V(1)} \otimes \tilde{f}_{\text{gb}}^{(0)} + \kappa P_{\text{qg}}^{(0)} \otimes \tilde{f}_{\text{bu}}^{(10)} \, ,$$

$$\tilde{f}_{\text{g}\bar{\text{b}}}^{(22)} = -\frac{\kappa}{2} P_{\text{qg}}^{(0)} \otimes P_{\text{gq}}^{(0)} \otimes \tilde{f}_{\text{gb}}^{(0)} \, .$$

B Additional figures
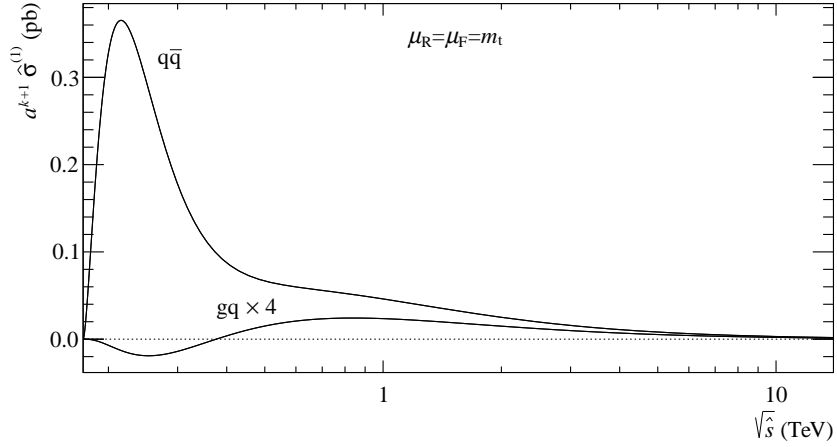
(a) *s*-channel production
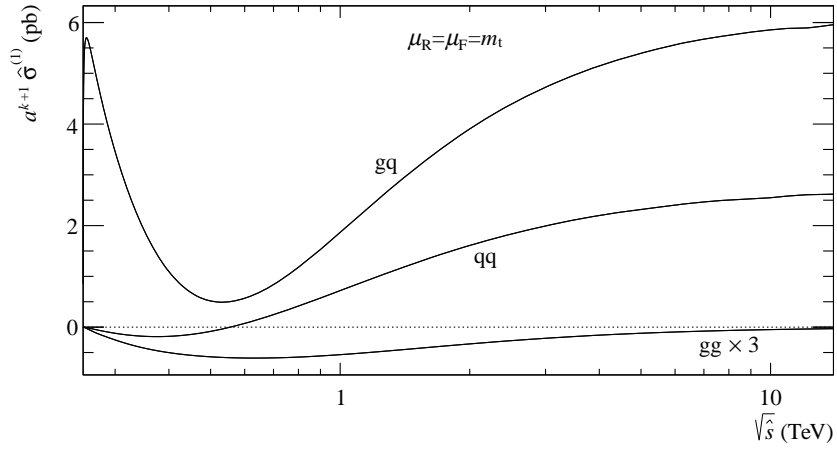
(b) Associated Wt production

Figure 10: NLO contributions to the partonic cross section for single top-quark production (*s*-channel, upper plot) (Wt channel, lower plot) as a function of the partonic centre-of-mass energy for a top-quark mass of 172.5 GeV. The scales μ_R and μ_F are set to the mass of the top quark. Here, q and $\bar{q}$ indicate all applicable flavours for the given channel.
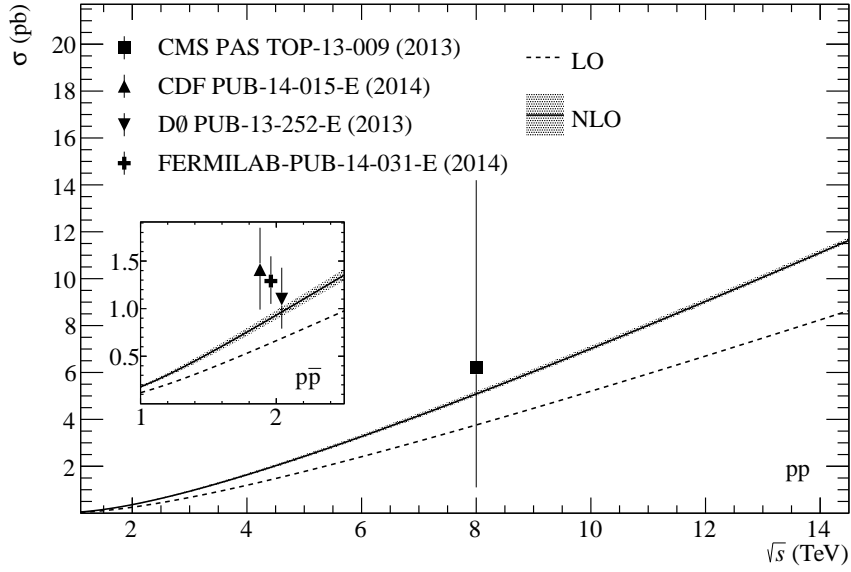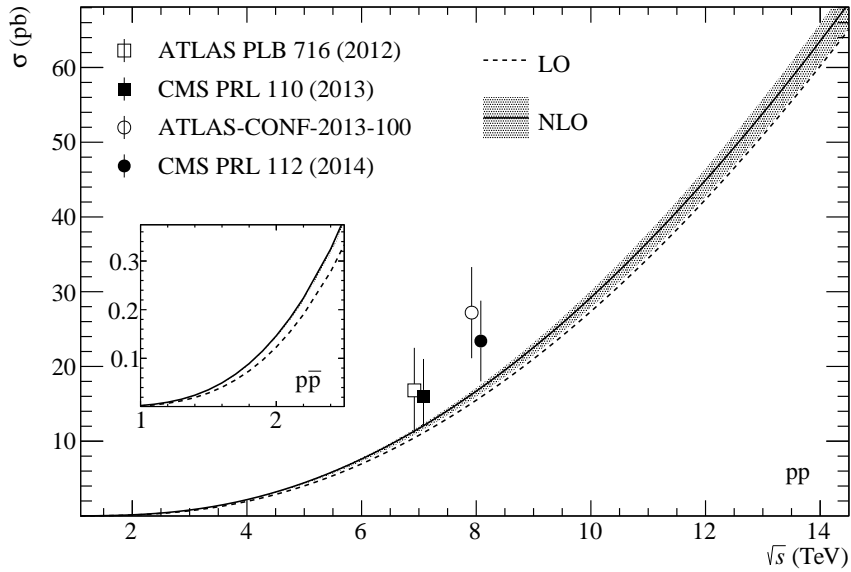
(a) *s*-channel production

(b) Associated Wt production

Figure 11: LO and NLO cross sections for single top-quark production calculated with the HATHOR program using CT10nlo as PDF set. The uncertainty band shown for NLO indicates the scale uncertainty. The latest measurements from CMS [40] and the Tevatron experiments [42,56,58] for *s*-channel production are shown for comparison, as well as measurements from the LHC for associated Wt production [37–39, 57].
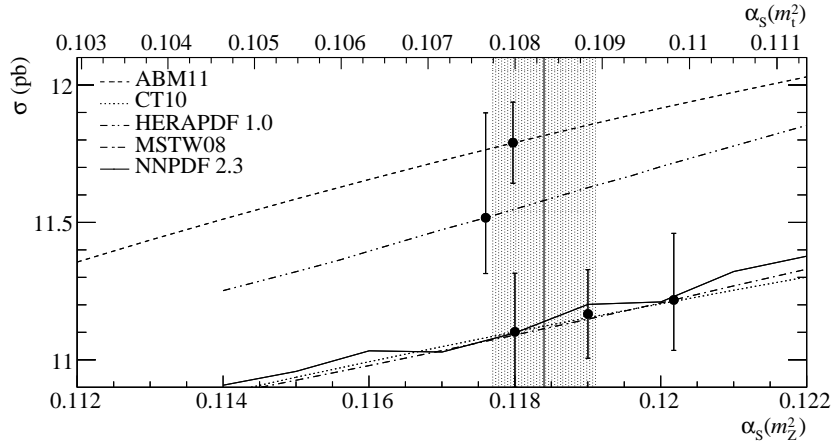
(a) *s*-channel production
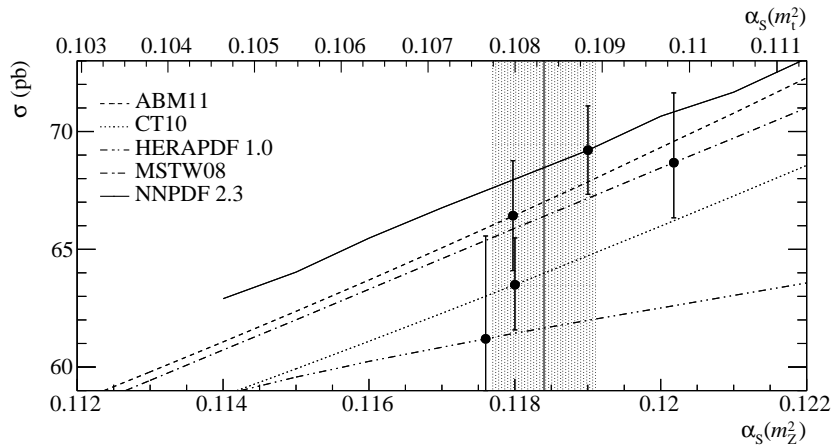
(b) Associated Wt production

Figure 12: Single top-quark cross sections for the *s*-channel and Wt production in NLO for different values of α_s, computed for different NLO PDFs at $\sqrt{s} = 14\,\mathrm{TeV}$ in pp scattering. For each PDF set, the best fit value and the corresponding full PDF uncertainty is indicated by the black marker and the error bar. The α_s values are given with respect to the mass of the Z boson (lower abscissa) and the mass of the top quark (upper abscissa). The vertical line and the shaded box represent the latest world average value of α_s and its uncertainty at the Z pole [51].

C Parametrization of the top-quark mass dependence

			ABM11			CT10			MSTW08			NNPDF2.3		
			$\sigma(\bar{m}_t)$	A	B	$\sigma(\bar{m}_t)$	A	B	$\sigma(\bar{m}_t)$	A	B	$\sigma(\bar{m}_t)$	A	B
t	$\sqrt{s}=8\,\mathrm{TeV}$	t	NLO	59.2705	-1.6541	1.569	53.5662	-1.6082	1.507	55.1053	-1.5995	1.492	55.2394	-1.5932	1.479
		s	NLO	3.48131	-3.8849	7.579	3.26836	-3.8673	7.526	3.28661	-3.8479	7.470	3.28760	-3.8561	7.496
		Wt	NLO	7.99547	-3.1930	5.61	8.34988	-2.9994	4.591	9.9572	-3.4	4.590	9.12887	-3.118	4.637
	$\sqrt{s}=14\,\mathrm{TeV}$	t	NLO	169.820	-1.3728	1.167	151.9990	-1.3468	1.135	155.3376	-1.3388	1.124	155.844	-1.3288	1.108
		s	NLO	7.33867	-3.6827	6.997	6.85043	-3.6681	6.954	6.83761	-3.6575	6.924	6.84724	-3.6505	6.906
		Wt	NLO	33.2384	-2.7747	4.46	31.7690	-2.6608	3.795	34.3656	-2.6566	3.785	34.6014	-2.6496	3.791
$\bar{t}$	$\sqrt{s}=8\,\mathrm{TeV}$	t	NLO	29.8380	-1.7837	1.785	28.6143	-1.6984	1.655	30.786	-1.6977	1.650	30.3703	-1.6831	1.624
		s	NLO	1.88127	-4.1505	8.396	1.82204	-4.1082	8.266	1.89441	-4.929	8.215	1.89198	-4.774	8.173
		Wt	NLO	7.94316	-3.1945	5.65	8.29082	-3.3	4.593	9.3557	-3.15	4.593	9.7282	-3.128	4.639
	$\sqrt{s}=14\,\mathrm{TeV}$	t	NLO	97.1989	-1.4759	1.314	90.3780	-1.4234	1.244	94.5101	-1.4187	1.235	94.8198	-1.4029	1.211
		s	NLO	4.46678	-3.8838	7.590	4.26563	-3.8531	7.499	4.39473	-3.8378	7.451	4.36731	-3.8230	7.414
		Wt	NLO	33.537	-2.7755	4.48	31.5711	-2.6616	3.797	34.1677	-2.6573	3.786	34.4158	-2.6503	3.792

Table 3: Coefficients for fast cross section evaluations using Eq. (41). All cross section values are given in pb. We use always NLO PDFs. The reference top-quark mass $\bar{m}_t$ used here is the current world average of 173.5 GeV [51].

D Example of HATHOR usage

```
#include "Hathor.h"
#include <iostream>

using namespace std;

int main() {
  Lhapdf pdf("CT10nlo");
  HathorSgTopT hathor(pdf);
  hathor.setColliderType(SgTop::PP);
  hathor.setSqrtShad(14000.);
  hathor.setScheme(SgTop::LO | SgTop::NLO);
  hathor.setPrecision(SgTop::LOW);

  double mt = 173., muf = mt, mur = mt;
  hathor.getXsection(mt, mur, muf);

  double val, err;
  hathor.getResult(0, val, err);
  cout << "cross section = (" << val << " +/- " << err << ") pb" << endl;

  return 0;
}
```

References

[1] T. Tait and C. Yuan, *Single Top Quark Production as a Window to Physics Beyond the Standard Model*, Phys. Rev. **D63** (2000) 014018, `arXiv:hep-ph/0007298`.

[2] J. Alwall, R. Frederix, J. Gerard, A. Giammanco, M. Herquet, et al., *Is $V_{tb} \approx 1$?*, Eur. Phys. J. **C49** (2007) 791–801, `arXiv:hep-ph/0607115 [hep-ph]`.

[3] G. Bordes and B. van Eijk, *Calculating QCD Corrections to Single Top Production in Hadronic Interactions*, Nucl. Phys. **B435** (1995) 23–58.

[4] T. Stelzer, Z. Sullivan, and S. Willenbrock, *Single Top Quark Production via W-Gluon Fusion at Next-To-Leading Order*, Phys. Rev. **D56** (1997) 5919–5927, `arXiv:hep-ph/9705398 [hep-ph]`.

[5] T. Stelzer, Z. Sullivan, and S. Willenbrock, *Single Top Quark Production at Hadron Colliders*, Phys. Rev. **D58** (1998) 094021, `arXiv:hep-ph/9807340 [hep-ph]`.

[6] B. Harris, E. Laenen, L. Phaf, Z. Sullivan, and S. Weinzierl, *The Fully Differential Single Top Quark Cross-Section in Next to Leading Order QCD*, Phys. Rev. **D66** (2002) 054024, `arXiv:hep-ph/0207055 [hep-ph]`.

[7] Z. Sullivan, *Understanding Single-Top-Quark Production and Jets at Hadron Colliders*, Phys. Rev. **D70** (2004) 114012, `arXiv:hep-ph/0408049 [hep-ph]`.

[8] Z. Sullivan, *Angular Correlations in Single-Top-Quark and Wjj Production at Next-To-Leading Order*, Phys. Rev. **D72** (2005) 094034, `arXiv:hep-ph/0510224 [hep-ph]`.

[9] J. Campbell, R. Ellis, and F. Tramontano, *Single Top Production and Decay at Next-To-Leading Order*, Phys. Rev. **D70** (2004) 094012, `arXiv:hep-ph/0408158 [hep-ph]`.

[10] Q. Cao and C.-P. Yuan, *Single Top Quark Production and Decay at Next-To-Leading Order in Hadron Collision*, Phys. Rev. **D71** (2005) 054022, `arXiv:hep-ph/0408180 [hep-ph]`.

[11] Q. Cao, R. Schwienhorst, J. Benitez, R. Brock, and C.-P. Yuan, *Next-To-Leading Order Corrections to Single Top Quark Production and Decay at the Tevatron: 2. t-Channel Process*, Phys. Rev. **D72** (2005) 094027, `arXiv:hep-ph/0504230 [hep-ph]`.

[12] S. Frixione, E. Laenen, P. Motylinski, and B. Webber, *Single-Top Production in MC@NLO*, JHEP **0603** (2006) 092, `arXiv:hep-ph/0512250 [hep-ph]`.

[13] S. Alioli, P. Nason, C. Oleari, and E. Re, *NLO Single-Top Production Matched with Shower in* POWHEG*: s- and t-Channel Contributions*, JHEP **0909** (2009) 111, `arXiv:0907.4076 [hep-ph]`.

[14] W. Giele, S. Keller, and E. Laenen, *QCD Corrections to W Boson Plus Heavy Quark Production at the Tevatron*, Phys. Lett. **B372** (1996) 141–149, `arXiv:hep-ph/9511449 [hep-ph]`.

[15] S. Zhu, *Next-To-Leading Order QCD Corrections to $bg \to tW^-$ at the CERN Large Hadron Collider*, Phys. Lett. **B524** (2002) 283–288.

[16] C. White, S. Frixione, E. Laenen, and F. Maltoni, *Isolating Wt Production at the LHC*, JHEP **0911** (2009) 074, `arXiv:0908.0631 [hep-ph]`.

[17] T. M. Tait, *The tW^- Mode of Single Top Production*, Phys. Rev. **D61** (2000) 034001, `arXiv:hep-ph/9909352 [hep-ph]`.

[18] J. Campbell and F. Tramontano, *Next-To-Leading Order Corrections to Wt Production and Decay*, Nucl. Phys. **B726** (2005) 109–130, `arXiv:hep-ph/0506289 [hep-ph]`.

[19] S. Frixione, E. Laenen, P. Motylinski, B. R. Webber, and C. D. White, *Single-Top Hadroproduction in Association with a W Boson*, JHEP **0807** (2008) 029, `arXiv:0805.3067 [hep-ph]`.

[20] E. Re, *Single-Top Wt-Channel Production Matched with Parton Showers Using the* POWHEG *Method*, Eur. Phys. J. **C71** (2011) 1547, `arXiv:1009.2450 [hep-ph]`.

[21] M. Smith and S. Willenbrock, *QCD and Yukawa Corrections to Single Top Quark Production via $q\bar{q} \to t\bar{b}$*, Phys. Rev. **D54** (1996) 6696–6702, arXiv:hep-ph/9604223 [hep-ph].

[22] Q. Cao, R. Schwienhorst, and C.-P. Yuan, *Next-To-Leading Order Corrections to Single Top Quark Production and Decay at Tevatron. 1. s-Channel Process*, Phys. Rev. **D71** (2005) 054023, arXiv:hep-ph/0409040 [hep-ph].

[23] J. Campbell, R. Frederix, F. Maltoni, and F. Tramontano, *Next-To-Leading-Order Predictions for t-Channel Single-Top Production at Hadron Colliders*, Phys. Rev. Lett. **102** (2009) 182003, arXiv:0903.0005 [hep-ph].

[24] J. Campbell, R. Frederix, F. Maltoni, and F. Tramontano, *NLO Predictions for t-Channel Production of Single Top and Fourth Generation Quarks at Hadron Colliders*, JHEP **0910** (2009) 042, arXiv:0907.3933 [hep-ph].

[25] S. Mrenna and C. Yuan, *Effects of QCD Resummation on $W^+ h$ and $t\bar{b}$ Production at the Tevatron*, Phys. Lett. **B416** (1998) 200–207, arXiv:hep-ph/9703224 [hep-ph].

[26] N. Kidonakis, *Single Top Production at the Tevatron: Threshold Resummation and Finite-Order Soft Gluon Corrections*, Phys. Rev. **D74** (2006) 114012, arXiv:hep-ph/0609287 [hep-ph].

[27] N. Kidonakis, *Higher-Order Soft Gluon Corrections in Single Top Quark Production at the LHC*, Phys.Rev. **D75** (2007) 071501, arXiv:hep-ph/0701080 [hep-ph].

[28] N. Kidonakis, *Two-Loop Soft Anomalous Dimensions for Single Top Quark Associated Production with a W^- Or H^-*, Phys. Rev. **D82** (2010) 054018, arXiv:1005.4451 [hep-ph].

[29] N. Kidonakis, *Next-To-Next-To-Leading Soft-Gluon Corrections for the Top Quark Cross Section and Transverse Momentum Distribution*, Phys. Rev. **D82** (2010) 114030, arXiv:1009.4935 [hep-ph].

[30] N. Kidonakis, *Next-To-Next-To-Leading-Order Collinear and Soft Gluon Corrections for t-Channel Single Top Quark Production*, Phys. Rev. **D83** (2011) 091503, arXiv:1103.2792 [hep-ph].

[31] M. Brucherseifer, F. Caola, and K. Melnikov, *On the NNLO QCD Corrections to Single-Top Production at the LHC*, arXiv:1404.7116 [hep-ph].

[32] M. Assadsolimani, P. Kant, B. Tausk, and P. Uwer, *Calculation of Two-Loop QCD Corrections for Hadronic Single Top-Quark Production in the t-Channel*, Phys.Rev. **D90** (2014) 114024, arXiv:1409.3654 [hep-ph].

[33] CDF Collaboration, *Observation of Electroweak Single-Top Quark Production*, Phys. Rev. Lett. **103** (2009) 092002, arXiv:0903.0885 [hep-ex].

[34] D0 Collaboration, *Observation of Single Top-Quark Production*, Phys. Rev. Lett. **103** (2009) 092001, arXiv:0903.0850 [hep-ex].

[35] ATLAS Collaboration, *Measurement of the t-Channel Single Top-Quark Production Cross Section in pp Collisions at* $\sqrt{s}=7\,TeV$ *with the ATLAS Detector*, Phys. Lett. **B717** (2012) 330–35, `arXiv:1205.3130 [hep-ex]`.

[36] CMS Collaboration, *Measurement of the Single-Top-Quark t-Channel Cross Section in pp Collisions at* $\sqrt{s}=7\,TeV$, JHEP **1212** (2012) 035, `arXiv:1209.4533 [hep-ex]`.

[37] CMS Collaboration, *Evidence for Associated Production of a Single Top Quark and W Boson in pp Collisions at* $\sqrt{s}=7\,TeV$, Phys. Rev. Lett. **110** (2013) 022003, `arXiv:1209.3489 [hep-ex]`.

[38] ATLAS Collaboration, *Evidence for the Associated Production of a W Boson and a Top Quark in ATLAS at* $\sqrt{s}=7\,TeV$, Phys. Lett. **B716** (2012) 142–159, `arXiv:1205.5764 [hep-ex]`.

[39] CMS Collaboration, *Observation of the Associated Production of a Single Top Quark and a W Boson in pp Collisions at sqrts* $=8\,TeV$, Phys. Rev. Lett. **112** (2014) 231802, `arXiv:1401.2942 [hep-ex]`.

[40] CMS Collaboration, *Search for s-Channel Single Top-Quark Production in pp Collisions at* $\sqrt{s}=8\,TeV$. CMS-PAS-TOP-13-009, 2013. `https://cds.cern.ch/record/1633190`.

[41] ATLAS Collaboration, *Search for s-Channel Single Top-Quark Production in pp Collisions at* $\sqrt{s}=7\,TeV$. ATLAS-CONF-2011-118, 2011. `https://cds.cern.ch/record/1376410`.

[42] CDF and D0 collaborations, *Observation of s-Channel Production of Single Top Quarks at the Tevatron*, Phys. Rev. Lett. (2014) , `arXiv:1402.5126 [hep-ex]`.

[43] J. Campbell and R. Ellis, *MCFM for the Tevatron and the LHC*, Nucl.Phys.Proc.Suppl. **205-206** (2010) 10–15, `arXiv:1007.3492 [hep-ph]`.

[44] M. Aliev, H. Lacker, U. Langenfeld, S. Moch, P. Uwer, et al., HATHOR*: HAdronic Top and Heavy quarks crOss section calculatoR*, Comput. Phys. Commun. **182** (2011) 1034–1046, `arXiv:1007.1327 [hep-ph]`.

[45] V. Ahrens, A. Ferroglia, M. Neubert, B. Pecjak, and L.-L. Yang, *RG-Improved Single-Particle Inclusive Cross Sections and Forward-Backward Asymmetry in* $t\bar{t}$ *Production at Hadron Colliders*, JHEP **1109** (2011) 070, `arXiv:1103.0550 [hep-ph]`.

[46] M. Czakon and A. Mitov, *Top++: A Program for the Calculation of the Top-Pair Cross-Section at Hadron Colliders*, `arXiv:1112.5675 [hep-ph]`.

[47] M. Beneke, P. Falgari, S. Klein, J. Piclum, C. Schwinn, et al., *Inclusive Top-Pair Production Phenomenology with TOPIXS*, JHEP **1207** (2012) 194, `arXiv:1206.2454 [hep-ph]`.

[48] S. Catani and M. Seymour, *A General Algorithm for Calculating Jet Cross-Sections in NLO QCD*, Nucl. Phys. **B485** (1997) 291–419, `arXiv:hep-ph/9605323 [hep-ph]`.

[49] S. Catani, S. Dittmaier, M. Seymour, and Z. Trocsanyi, *The Dipole Formalism for Next-To-Leading Order QCD Calculations With Massive Partons*, Nucl. Phys. **B627** (2002) 189–265, `arXiv:hep-ph/0201036 [hep-ph]`.

[50] T. Carli, D. Clements, A. Cooper-Sarkar, C. Gwenlan, G. P. Salam, F. Siegert, P. Starovoitov and M. Sutton, *A posteriori inclusion of parton density functions in NLO QCD final-state calculations at hadron colliders: The APPLGRID Project*, Eur. Phys. J. C **66** (2010) 503, `arXiv:0911.2985 [hep-ph]`.

[51] Particle Data Group Collaboration, J. Beringer et al., *Review of Particle Physics (RPP)*, Phys.Rev. **D86** (2012) 010001.

[52] M. Whalley, D. Bourilkov, and R. Group, *The Les Houches Accord PDFs (LHAPDF) and LHAGLUE*, `arXiv:hep-ph/0508110 [hep-ph]`. `http://hepforge.cedar.ac.uk/lhapdf/`.

[53] ATLAS Collaboration, *Measurement of the Inclusive and Fiducial Cross-Section of Single Top-Quark t-Channel Events in pp Collisions at $\sqrt{s} = 8\,TeV$*. ATLAS-CONF-2014-007, 2014. `https://cds.cern.ch/record/1668960`.

[54] CMS Collaboration, *Measurement of the t-Channel Single-Top-Quark Production Cross Section and of the $|V_{tb}|$ CKM Matrix Element in pp Collisions at $\sqrt{s} = 8\,TeV$*. CMS-TOP-12-038-3, 2014. Accepted by JHEP.

[55] CDF Collaboration, *Measurement of Single Top Quark Production in $7.5\,fb^{-1}$ of CDF Data Using Neural Networks*. CDF/PUB/TOP/PUBLIC/10793, 2013.

[56] D0 Collaboration, *Evidence for s-Channel Single Top Quark Production in $p\bar{p}$ Collisions at $\sqrt{s} = 1.96\,TeV$*. FERMILAB-PUB-13-252-E, 2013.

[57] ATLAS Collaboration, *Measurement of the Cross-Section for Associated Production of a Top Quark and a W Boson at $\sqrt{s} = 8\,TeV$ with the ATLAS detector*. ATLAS-CONF-2013-100, 2013. `https://cds.cern.ch/record/1600799`.

[58] CDF Collaboration, *Evidence for s-Channel Single-Top-Quark Production in Events with one Charged Lepton and two Jets at CDF*, Phys. Rev. Lett. (2014) , `arXiv:1402.0484 [hep-ex]`. Accepted by PRL.

[59] S. Alekhin, J. Blumlein, and S. Moch, *Parton Distribution Functions and Benchmark Cross Sections at NNLO*, Phys.Rev. **D86** (2012) 054009, `arXiv:1202.2281 [hep-ph]`.

[60] H.-L. Lai, M. Guzzi, J. Huston, Z. Li, P. M. Nadolsky, et al., *New Parton Distributions for Collider Physics*, Phys. Rev. **D82** (2010) 074024, `arXiv:1007.2241 [hep-ph]`.

[61] A. Martin, W. Stirling, R. Thorne, and G. Watt, *Parton Distributions for the LHC*, Eur.Phys.J. **C63** (2009) 189–285, `arXiv:0901.0002 [hep-ph]`.

[62] R. Ball, V. Bertone, S. Carrazza, C. Deans, L. Del Debbio, et al., *Parton Distributions with LHC Data*, Nucl.Phys. **B867** (2013) 244–289, `arXiv:1207.1303 [hep-ph]`.

[63] R. Ball, L. Del Debbio, S. Forte, A. Guffanti, J. Latorre, et al., *A First Unbiased Global NLO Determination of Parton Distributions and their Uncertainties*, Nucl.Phys. **B838** (2010) 136–206, `arXiv:1002.4407 [hep-ph]`.

[64] H1 and ZEUS collaborations, *Combined Measurement and QCD Analysis of the Inclusive* e^+p *Scattering Cross Sections at HERA*, JHEP **1001** (2010) 109, `arXiv:0911.0884 [hep-ex]`.